

# Asymmetric cell division during T cell development controls downstream fate

Kim Pham,<sup>1,3</sup> Raz Shimoni,<sup>1,3</sup> Mirren Charnley,<sup>1,3,4</sup> Mandy J. Ludford-Menting,<sup>1,3</sup> Edwin D. Hawkins,<sup>1</sup> Kelly Ramsbottom,<sup>1</sup> Jane Oliaro,<sup>1,7</sup> David Izon,<sup>8</sup> Stephen B. Ting,<sup>1</sup> Joseph Reynolds,<sup>9</sup> Grant Lythe,<sup>9</sup> Carmen Molina-Paris,<sup>9</sup> Heather Melichar,<sup>10</sup> Ellen Robey,<sup>10</sup> Patrick O. Humbert,<sup>2,5,6,7</sup> Min Gu,<sup>3</sup> and Sarah M. Russell<sup>1,3,5,7</sup>

<sup>1</sup>Immune Signalling Laboratory and <sup>2</sup>Cell Cycle and Cancer Genetics Laboratory, Peter MacCallum Cancer Centre, East Melbourne, Victoria 3002, Australia

<sup>3</sup>Centre for Micro-Photonics and <sup>4</sup>Industrial Research Institute Swinburne, Faculty of Science, Engineering, and Technology, Swinburne University of Technology, Hawthorn, Victoria 3122, Australia

<sup>5</sup>Department of Pathology, <sup>6</sup>Department of Biochemistry and Molecular Biology, and <sup>7</sup>Sir Peter MacCallum Department of Oncology, University of Melbourne, Parkville, Victoria 3010, Australia

<sup>8</sup>St. Vincent's Institute of Medical Research, Fitzroy, Victoria 3065, Australia

<sup>9</sup>Department of Applied Mathematics, School of Mathematics, University of Leeds, Leeds LS2 9JT, England, UK

<sup>10</sup>Division of Immunology and Pathogenesis, Department of Molecular and Cell Biology, University of California, Berkeley, Berkeley, CA 94720

During mammalian T cell development, the requirement for expansion of many individual T cell clones, rather than merely expansion of the entire T cell population, suggests a possible role for asymmetric cell division (ACD). We show that ACD of developing T cells controls cell fate through differential inheritance of cell fate determinants Numb and  $\alpha$ -Adaptin. ACD occurs specifically during the  $\beta$ -selection stage of T cell development, and subsequent divisions are predominantly symmetric. ACD is controlled by interaction with stromal cells and chemokine receptor signaling and uses a conserved network of polarity regulators. The disruption of polarity by deletion of the polarity regulator, Scribble, or the altered inheritance of fate determinants impacts subsequent fate decisions to influence the numbers of DN4 cells arising after the  $\beta$ -selection checkpoint. These findings indicate that ACD enables the thymic microenvironment to orchestrate fate decisions related to differentiation and self-renewal.

## Introduction

The expansion and differentiation of cells during development and homeostasis often involves asymmetric cell division (ACD), in which a cell divides asymmetrically to produce two daughter cells with different fate potential. ACD underpins many aspects of *Caenorhabditis elegans* and *Drosophila melanogaster* development, including facilitating the expansion of populations of cells during development, enabling many founder cells to con-

tribute several progeny to the final population (Knoblich, 2010; Losick et al., 2011). Recent findings have suggested that ACD plays a less important role in creating population-level diversity in mammalian tissues, where individual clones can dominate the population (Verzi and Shivdasani, 2010; Simons and Clevers, 2011; Edgar, 2012). In contrast to expansion of populations such as those arising from the intestinal crypt (Simons and Clevers, 2011; Blanpain and Fuchs, 2014), expansion and differentiation of individual clones during development of T and B cells of the adaptive immune system is particularly important because each clone contains genetically different receptors for antigen. This opens the possibility that ACD might be required to facilitate control at the clonal level. Cells of hematopoietic origin, including hematopoietic stem cells and immune cells such as mature B and T cells, can undergo ACD, but the role of ACD in immune cell development is not known (Chang et al., 2007, 2011; Oliaro et al., 2010; Barnett et al., 2012; King et al., 2012; Thauinat et al., 2012; Ting et al., 2012; Buchholz et al., 2013; Gerlach et al.,

Correspondence to Sarah M. Russell: sarah.russell@petermac.org

K. Pham's present address is Immunology Division, Walter and Eliza Hall Institute, Parkville, Victoria 3052, Australia.

R. Shimoni's present address is iThree Institute, University of Technology Sydney, Ultimo, New South Wales 2007, Australia.

E.D. Hawkins' present address is Imperial College London, London SW72AZ, England, UK.

S.B. Ting's present address is Dept. of Haematology, Alfred Health and Stem Cell Research Group, Australian Centre for Blood Diseases, Monash University, Melbourne, Victoria 3800, Australia.

H. Melichar's present address is Maisonneuve-Rosemont Hospital Research Centre, Montreal, Quebec H1T 2M4, Canada.

Abbreviations used in this paper: ACD, asymmetric cell division; aPKC, atypical PKC; CTX, CellTrace violet; CXCR4, chemokine receptor type 4; DL1, Delta-like 1; Dlg, discs large; DN, double negative; DP, double positive; LAT, linker for activation of T cells; MTOC, microtubule organizing center; PR, polarization ratio; SCD, symmetric cell division; SP, single positive; TCR, T cell receptor.

© 2015 Pham et al. This article is distributed under the terms of an Attribution-Noncommercial-Share Alike-No Mirror Sites license for the first six months after the publication date (see <http://www.rupress.org/terms>). After six months it is available under a Creative Commons License (Attribution-Noncommercial-Share Alike 3.0 Unported license, as described at <http://creativecommons.org/licenses/by-nc-sa/3.0/>).

2013; Yamamoto et al., 2013; Arsenio et al., 2014; Pham et al., 2014; Zimdahl et al., 2014; Metz et al., 2015).

T cell development involves waves of proliferation intertwined with differentiation, apoptosis, and limited self-renewal to produce mature T cells that each express a unique T cell receptor (TCR). A checkpoint that has profound importance for subsequent immune function and prevention of leukemia is the  $\beta$ -selection checkpoint (Yui and Rothenberg, 2014). Developing T cells that enter the  $\beta$ -selection checkpoint orchestrate seemingly conflicting processes: genomic recombination for TCR rearrangement, cell proliferation with differentiation, and cell proliferation without differentiation (self-renewal). The developmental stages before and after the  $\beta$ -selection checkpoint are termed DN3a and DN3b stages, respectively, and the transition between these stages involves dramatic changes in transcriptional profile, with abrupt shutdown or initiation of key fate regulators (Yui and Rothenberg, 2014). Transition through the checkpoint also triggers a proliferative burst of six to eight divisions, changes in susceptibility to apoptosis, and subsequent differentiation into mature T cells (Aifantis et al., 2006; Koch and Radtke, 2011). Developing T cells traffic through the thymus in a highly regulated manner such that each stage resides in a different niche, which provides key environmental cues to control fate (Aifantis et al., 2006; Koch and Radtke, 2011). Recent evidence that cell competition within the thymus constrains self-renewal to prevent leukemia suggests that the provision of rate-limiting cues determines fate during T cell development (Martins et al., 2014). However, it is not yet known how these spatially constrained cues and signaling pathways converge to orchestrate progression through the  $\beta$ -selection checkpoint.

ACD, which influences fate in many cell types, involves the establishment and maintenance of polarity during division that results in two daughter cells with different molecular compositions and fates (Knoblich, 2010). ACD is regulated by polarity proteins such as atypical PKC (aPKC), discs large (Dlg), and Scribble and leads to the differential inheritance of fate determinants to regulate the development and homeostasis of the brain, muscle, gut, mammary gland, and skin (Li, 2013; Paridaen and Huttner, 2014). In support of the notion that thymocytes might undergo ACD, thymocyte differentiation requires the polarity protein, Scribble, and there is some evidence that Numb is polarized during thymocyte division (Aguado et al., 2010; Pike et al., 2011). Given the requirement for each clone to be represented in the final population, we proposed that ACD might play an important role during the  $\beta$ -selection checkpoint of T cell development. We show here that ACD occurs specifically during the  $\beta$ -selection checkpoint of T cell development at the DN3a stage to influence subsequent fate decisions and that this is regulated via interactions with stromal cells. The control and impact of ACD during  $\beta$  selection parallels many characteristics of ACD previously found in *D. melanogaster* and *C. elegans* model systems and offers a new mammalian model with unique opportunities for elucidating how ACD controls cell fate.

## Results

### DN3 thymocytes asymmetrically localize polarity proteins and cell fate determinants during interphase

We first used an in vitro system of T cell development whereby progenitor cells are cultured on a stromal cell line that stably ex-

presses the Notch ligand Delta-like 1 (OP9-DL1). This is a tractable system of T cell development that recapitulates almost all aspects of development and lineage commitment from thymocytes to mature T cells particularly at the  $\beta$ -selection checkpoint (Schmitt and Zúñiga-Pflücker, 2002). To determine whether thymocytes at the DN3  $\beta$ -selection checkpoint exhibit cell polarity and whether thymic stromal cells provide a cue for polarity, we performed immunofluorescence microscopy to assess the localization of  $\alpha$ -tubulin on fixed DN3 thymocytes (comprised of DN3a and DN3b cells, which represent the stages before and after the  $\beta$ -selection checkpoint, respectively) that had been generated by culture of fetal liver hematopoietic precursors on the OP9-DL1 stromal cell line. To assess polarity in relation to the stromal cells, DN3 thymocytes were costained for polarity and cell fate proteins, and thymocytes with a microtubule organizing center (MTOC) polarized to the stromal cell interface were scored for protein polarization where polarization was defined as a clear enrichment of fluorescence at the interface with the stromal cell (Fig. 1). To validate this scoring approach, Notch1 polarization was quantified by manually dividing the image of the cell in half along the axis perpendicular to the interface and measuring the fluorescence in each hemisphere (Fig. S1). This method showed clear polarization of Notch1 to the hemisphere closest to the stromal cell, but not of the control protein CD25. Similarly, blind scoring demonstrated strong polarization of the cell fate determinant, Notch1, to the interface with the stromal cell in 83% of thymocyte–stromal conjugates (Fig. 1 and Fig. S1). The regulator of Notch, Numb, was also clearly polarized, and  $\alpha$ -Adaptin, previously shown to regulate ACD of hematopoietic stem cells (Ting et al., 2012), displayed both polarized and nonpolarized distributions (Fig. 1). Polarity proteins such as aPKC, Scribble, and Dlg displayed a variety of localization patterns, although none as striking as Notch and Numb. These mixed polarization patterns possibly reflected different stages of interaction with stromal cells and are compatible with the transient movement of polarity proteins observed during interaction of T cells with antigen-presenting cells (Xavier et al., 2004; Ludford-Menting et al., 2005; Oliaro et al., 2006, 2010; Gérard et al., 2007; Real et al., 2007). Expression during T cell development of mRNA for these proteins was also confirmed using the Immunological Genome Database (Fig. S2; Heng et al., 2008). Collectively, these results demonstrate that DN3 thymocytes possess intracellular polarity, which appears to be regulated by interactions with stromal cells.

### Asymmetric partitioning of $\alpha$ -Adaptin and Numb during DN3 thymocyte division

We focused on two molecules,  $\alpha$ -Adaptin and Numb, both endocytic regulators of cell fate that were previously observed to be polarized during ACD in other developmental systems.  $\alpha$ -Adaptin induces hematopoietic stem cell self-renewal in vivo upon sequential transplantation assays and is segregated asymmetrically in ~25% of dividing hematopoietic stem cells (Ting et al., 2012). Numb regulates Notch vesicular trafficking and signaling during ACD, and Notch is required for thymocyte survival during the  $\beta$ -selection checkpoint (Ciofani and Zúñiga-Pflücker, 2005; Koch and Radtke, 2011; Couturier et al., 2012). DN3 thymocytes were cultured overnight on OP9-DL1 stromal cells, fixed, and stained for tubulin, DNA, and  $\alpha$ -Adaptin or Numb. Dividing DN3 thymocytes were identified on the basis of nuclear shape and the presence of a mitotic spindle, and the distribution of  $\alpha$ -Adaptin

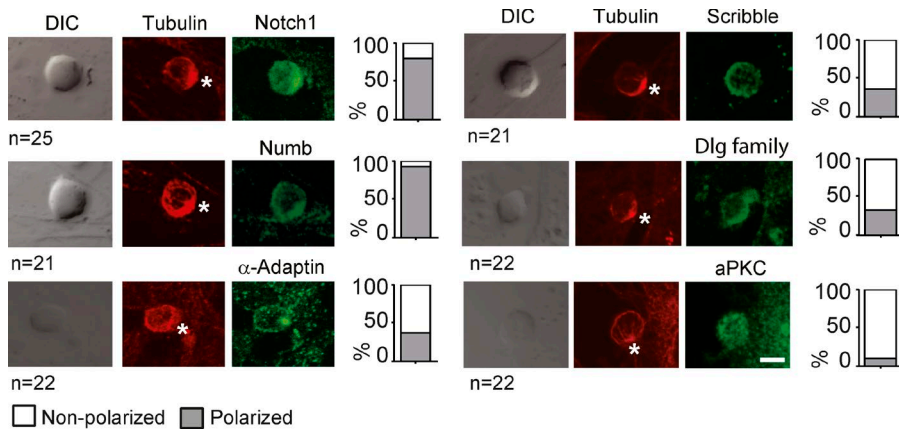


**Figure 1. DN3 thymocytes polarize during stromal interactions at interphase.** DN3 thymocytes express and polarize cell fate and polarity proteins. DN3–stromal cell conjugates were fixed and costained with  $\alpha$ -tubulin (red) and either a cell fate or polarity protein (green). Only cells in which the MTOC was recruited to the stromal interface were analyzed. Of these, the percentage of thymocytes is shown displaying polarized localization if the protein of interest recruited to the stromal interface (gray bars), or nonpolarized localization if it did not colocalize with the MTOC at the thymocyte–stromal interface. The asterisks indicate the interface between the thymocyte and stromal cell. Bar, 10  $\mu$ m.  $n = 2$  independent experiments;  $n = 21$ – $25$  for each condition. DIC, differential interference contrast. Also see Fig. S2 for microarray analysis of expression of polarity proteins and cell fate determinants in the different stages of T cell development.

and Numb was scored as asymmetric or symmetric based on blinded operator assessment of fluorescence distribution.  $\alpha$ -Adaptin and Numb were asymmetric in 17.6% and 12.0%, respectively, of dividing DN3 thymocytes during late mitosis (Fig. 2 A). These data suggest that some DN3 thymocytes polarize fate determinants during division, prompting further efforts to quantify polarity.

To quantify the extent of asymmetry of  $\alpha$ -Adaptin and Numb during division, we used time-lapse microscopy and a custom image analysis platform, TACTICS (Shimoni et al., 2013). DN3 thymocytes transduced with Cherry-tagged  $\alpha$ -Adaptin and GFP were cultured on OP9-DL1 stromal cells, imaged in cell paddocks (Day et al., 2009), and subjected to image processing methods that we had previously developed for identification of divisions and quantification of polarity (Pham et al., 2013; Shimoni et al., 2013). Cells were reoriented in silico using the long axis as a reference, and images from sequential frames were compressed onto a line of single-pixel width. This temporal analysis indicated that cell polarization was sustained during and after division (Fig. 2 B and Fig. S3 A). These data provide reassurance that the polarization observed in the mitotic cells was not an artifact of the imaging, but genuine asymmetry that was transmitted to the daughter cells. The absolute polarization ratios (PRs; calculated as the difference in fluorescence between the two halves divided by the sum of the fluorescence; Oliaro et al., 2010; Pham et al., 2013) of Cherry- $\alpha$ -Adaptin and GFP were calculated for 51 DN3 divisions (Fig. 2 C). The PR was significantly greater for Cherry- $\alpha$ -Adaptin than for the GFP control ( $P < 0.0005$ ) but was not uniform within the population, with the PR for Cherry- $\alpha$ -Adaptin ranging from 0 to 0.76, indicating that some, but not all, of the cells were asymmetric. The extent of polarity, per se, does not indicate which divisions should be classified as symmetric cell division (SCD) or ACD, but it is common practice, particularly in studies of hematopoietic ACD, to arbitrarily designate a cutoff value with which to artificially categorize events as ACD or SCD so that comparisons can be made between proteins or populations of cells (Chang et al., 2007; Wu et al., 2007). For this purpose, in this study we assigned a cutoff PR value of 0.27 based on the spread of control PR. A cutoff PR value of 0.27 yielded  $<1\%$  ACD for negative control data from all the experiments combined and discriminated between two reasonably distinct groups of PRs for our first two

test proteins. Thus, 0.27 was used as a cutoff for all subsequent analyses (Fig. S3 B). With this cutoff, 21.6% of DN3 cells were ascribed as polarized for Cherry- $\alpha$ -Adaptin (ACD events), compared with 2% for GFP control. Similarly, DN3 thymocytes showed significantly greater polarization of GFP-Numb compared with Cherry control ( $P < 0.0001$ ), which was sustained beyond cell division (Fig. 2, B and C, top), and the same cutoff yielded 0% ACD for the control and 12.7% ACD for GFP-Numb (Fig. 2 C, middle). Polarization of  $\alpha$ -Adaptin and Numb in dividing DN3 cells contrasted with GFP-LAT (linker for activation of T cells), a TCR-associated molecule that served here as a negative control and yielded 0% ACD events (Fig. 2 C, bottom). These data indicate that  $\alpha$ -Adaptin and Numb, but not LAT or GFP and Cherry controls, were polarized before, during, and after DN3 division. Collectively, DN3 thymocytes exhibit both symmetric and asymmetric distribution of Numb and  $\alpha$ -Adaptin during division, and asymmetry is sustained after DN3 division.

Given that asymmetry of cell fate determinants such as Numb and  $\alpha$ -Adaptin was only observed in a small proportion of DN3 divisions, it was possible that the mode of DN3 division (asymmetric or symmetric) depended on the stage of differentiation. Whether or not DN3a cells undergo cell division has been unclear until recently (Kreslavsky et al., 2012), so we assessed whether purified DN3a cells remained as DN3a after cell divisions using CellTrace violet (CTV) labeling and indeed found that DN3a thymocytes were able to undergo at least one division before becoming DN3b thymocytes (Fig. S3 C). To investigate whether asymmetry preferentially occurred at the DN3a stage before  $\beta$  selection, or at the DN3b stage after  $\beta$  selection, DN3a and DN3b thymocytes were sorted based on CD28 expression, recultured on OP9-DL1 stromal cells for 12 to 15 h, fixed, and stained for endogenous  $\alpha$ -Adaptin as a marker of polarity. 44.5% of the DN3a thymocytes polarized  $\alpha$ -Adaptin during division compared with 15.6% of dividing DN3b cells (Fig. 2 D). This difference was not a result of the process of DN3a isolation because DN3a cells that were cultured for 48 h (by which time most have differentiated to the DN3b stage) showed only 17.1% ACD (Fig. 2 D). There is still the possibility that ACD occurs at early or late cell divisions of the DN3a stage, but together, these data indicate that asymmetry during division occurs preferentially at the DN3a stage.



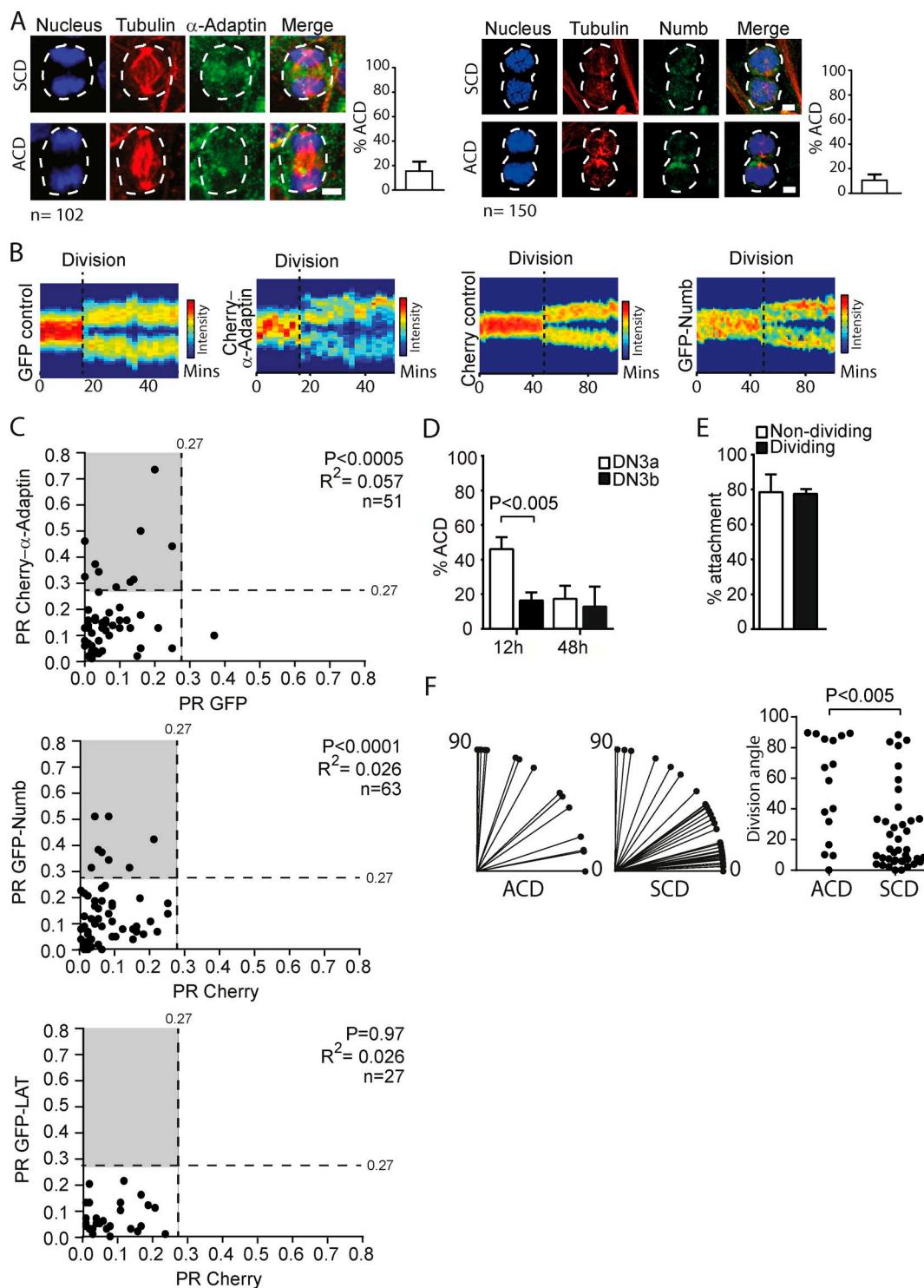


**Figure 2. DN3 thymocytes undergo ACD.** (A) A proportion of DN3 thymocytes asymmetrically localizes  $\alpha$ -Adaptin and Numb during division. Z-projected images of dividing DN3 thymocytes cultured on OP9-DL1 stromal cells, fixed, and stained for  $\alpha$ -tubulin, DNA, and either  $\alpha$ -Adaptin or Numb. Images were scored as SCD or ACD based on subjective operator assessment of fluorescence distribution (the operator was blinded as to the identity of each stain). Scores are shown as percentages and analyzed from  $n = 3$  independent experiments;  $n = 102$  ( $\alpha$ -Adaptin) and 150 (Numb). The white dotted lines depict the outline of the dividing thymocyte. Bars, 10  $\mu$ m. (B) Asymmetry is maintained beyond division. Heat map projection of both GFP and Cherry- $\alpha$ -Adaptin (left) or Cherry and GFP-Numb (right) in a DN3 thymocyte tracked before and after division. The black dotted line indicates the time of cytokinesis. Scale of absolute units of fluorescence intensity is shown. (C) Absolute PR plots in dividing DN3 thymocytes expressing GFP and Cherry- $\alpha$ -Adaptin (top), Cherry and GFP-Numb (middle), and Cherry and GFP-LAT (bottom). Absolute PR is calculated as the absolute difference in fluorescence between the two halves divided by the sum of fluorescence.  $n = 3$  independent experiments. Total number of analyzed divisions: Cherry- $\alpha$ -Adaptin,  $n = 51$ ; GFP-Numb,  $n = 63$ ; and GFP-LAT,  $n = 27$ . A paired  $t$  test comparing PR values for test and control protein and Pearson's linear correlation coefficient are shown. (D) DN3a thymocytes preferentially undergo ACD compared with DN3b thymocytes. DN3a and DN3b thymocytes were cultured on OP9-DL1 stromal cells stained for  $\alpha$ -tubulin and  $\alpha$ -Adaptin as a marker for asymmetry during division. The percentage of ACD events at 12 h and 48 h of culture as determined by polarization of  $\alpha$ -Adaptin during DN3a and DN3b division;  $n = 4$  independent experiments. (E) The majority of DN3 thymocytes interact with stromal cells

### Asymmetry during division of DN3 thymocytes is dictated by interaction with the stromal cell

During activation of mature T cells, polarity during ACD is dictated by contact with the antigen-presenting cell that bears a foreign peptide (Oliaro et al., 2006). We reasoned that stromal cells in vitro might provide a similar cue for thymocytes. To determine stromal interactions and orientation of dividing thymocytes, DN3 cells transduced with Cherry-tubulin were cultured with OP9-DL1 stromal cells and imaged. Before division, 78.5% of DN3 thymocytes were attached to the stromal cell, and the interaction was clearly sustained, as a similar proportion (77.6%) displayed attachment to the stromal cell during cell division (Fig. 2 E). The DN3 thymocytes divided in a variety of orientations, with the mitotic spindle orientated parallel to the interface in 25.5% of dividing cells and perpendicular to the interface in 32.1% of dividing cells (the other divisions were either burrowed under the stromal cell or not interacting; Fig. S4). These data indicate that DN3 thymocytes frequently interact with stromal cells during interphase and division, but do not always divide perpendicularly to the stromal cell. Given that only a proportion of the DN3a cells exhibited asymmetry at division (44.5% as per our arbitrary cutoff), we assessed whether the orientation of the mitotic spindle might correlate with asymmetry. Time-lapse videos of DN3 thymocytes transduced with GFP and Cherry- $\alpha$ -Adaptin were reassessed to determine the correlation between the orientation of division with respect to the stromal cells (assessed by comparing the angle between a line through the long axis of the dividing cell and a line along the stromal interface) and polarity at division (as defined by polarization of Cherry- $\alpha$ -Adaptin using the 0.27 cutoff to ascribe SCD and ACD). Remarkably, there was a striking difference in the angles of division, with more frequent perpendicular divisions for ACD than for SCD ( $P < 0.005$ ; Fig. 2 F). The increase in asymmetry when thymocytes divided perpendicular to the stromal cell indicates that stromal interactions might coordinate polarity with spindle orientation. Importantly, these findings indicate that polarity of DN3a cells at division is not a result of stochastic distribution of the protein, but is actively coordinated by extrinsic stromal interactions, meeting the requirements for ACD.

### Signaling through the chemokine receptor CXCR4 is required for ACD in DN3 thymocytes

Having identified a role for the stromal cell in thymocyte ACD, we asked what molecular cue might be provided by the stromal cells to polarize DN3 thymocytes before and at division. Three cell surface receptors are known to regulate DN3 fate determination: pre-TCR, chemokine receptor type 4 (CXCR4), and Notch. Pre-TCR signaling is the defining event of the  $\beta$ -selection checkpoint and is triggered by effective recombination of the TCR- $\beta$  chain but is ligand independent (Ciofani et al., 2004), and so is unlikely to be regulated by stromal interactions. The CXCR4 ligand (CXCL12 or SDF1- $\alpha$ ) can be soluble or

presented by the stromal cell and induces thymocyte polarity (Plotkin et al., 2003; Janas et al., 2010), and Notch ligands must be provided by the stromal cell (Ciofani et al., 2004; Trampont et al., 2010). In fixed and stained DN3 thymocytes at interphase, blind scoring showed recruitment to the stromal interface for CXCR4 (50% of 150 thymocytes), similar to the previously observed polarization of Notch1 (83.3% of 150 thymocytes), but not CD25 (27.7% of 88 thymocytes; Fig. 3 A).

To begin determining possible external cues that might influence ACD, we focused on CXCR4 interactions with CXCL12 from the stromal cells. We used  $\alpha$ -Adaptin again as a marker of polarity to discern whether chemokine signaling through CXCR4 served as a polarity cue before ACD. DN3a thymocytes were cultured on OP9-DL1 stromal cells, fixed, and stained for tubulin and  $\alpha$ -Adaptin. Disrupting CXCR4 signaling with the specific inhibitor AMD3100 decreased the attachment of DN3a thymocytes to stromal cells as indicated by the number of cells that remained on the slide after staining (Fig. 3 B). Of the thymocytes that did interact, MTOC recruitment to the stromal cell was not significantly reduced, indicating that localization of the MTOC does not depend on CXCR4 signaling (Fig. 3 B). To determine whether ACD was reduced by treatment with the CXCR4 inhibitor, we stained DN3a divisions for either Numb or  $\alpha$ -Adaptin and assigned ACD or SCD based on blind scoring as in Fig. 2 A. First, as with the quantitative time-lapse imaging, polarity was greater for the fixed and stained DN3a cells than for the bulk DN3 cells with 56.7% of divisions scored as ACD for  $\alpha$ -Adaptin (Fig. 3 C) and 47.4% scored as ACD for Numb (Fig. 3 D; compare with 17.6% and 12.0%, respectively; Fig. 2 A). Second, polarity at division was reduced by the addition of AMD3100 for both  $\alpha$ -Adaptin and Numb ( $P < 0.05$ ), with 26.3% and 27.5% scored as ACD for  $\alpha$ -Adaptin and Numb, respectively (Fig. 3, C and D). The reduction in ACD correlated with decreased cell numbers, increased thymocyte death, and decreased differentiation to the double-positive (DP) stage (Fig. 3 E). These data indicate that CXCR4 signaling provides at least two functions with respect to stromal interactions. CXCR4 signaling facilitates recruitment to the stromal cell, and, once the thymocyte has docked on the stromal cell, CXCR4 provides a cue to promote  $\alpha$ -Adaptin and Numb polarization, suggesting that it is at least part of the polarity cue for ACD.

### Polarity at division correlates with functional downstream fates of daughter thymocytes

To begin to determine whether ACD of DN3a cells influences fate determination, we assessed whether alterations in polarization during division might correlate with alterations in fate using three approaches to disrupt polarity. Because ACD occurs preferentially at the DN3a stage, we considered that a functional role for ACD would be indicated by an alteration in progression from DN3 to DN4 and subsequent differentiation stages.

during interphase and division. Time-lapse imaging of DN3 thymocytes transduced with Cherry-tubulin were cultured on OP9-DL1 stromal cells, and the percent attachment of Cherry-tubulin DN3 thymocytes with stromal cells when not dividing or dividing are shown.  $n = 3$  independent experiments;  $n = 450$  (nondividing) and 78 (dividing). (F) Enrichment of perpendicular divisions in DN3 thymocytes undergoing ACD. Time-lapse imaging of DN3 thymocytes transduced with Cherry- $\alpha$ -Adaptin and GFP during culture on OP9-DL1 stromal cells. A line was drawn through the axis of division based on the center of each nascent daughter, and the angle of the spindle axis was calculated relative to a line through the interface with the stromal cell (depicted as the horizontal axis in the left plot). The angles were compiled in a scatter plot on the right.  $n = 3$  independent experiments and  $n = 54$  divisions. An unpaired Student's  $t$  test ( $P < 0.05$ ) was used. Data are represented as  $\pm$ SEM. Also see Fig. S4.

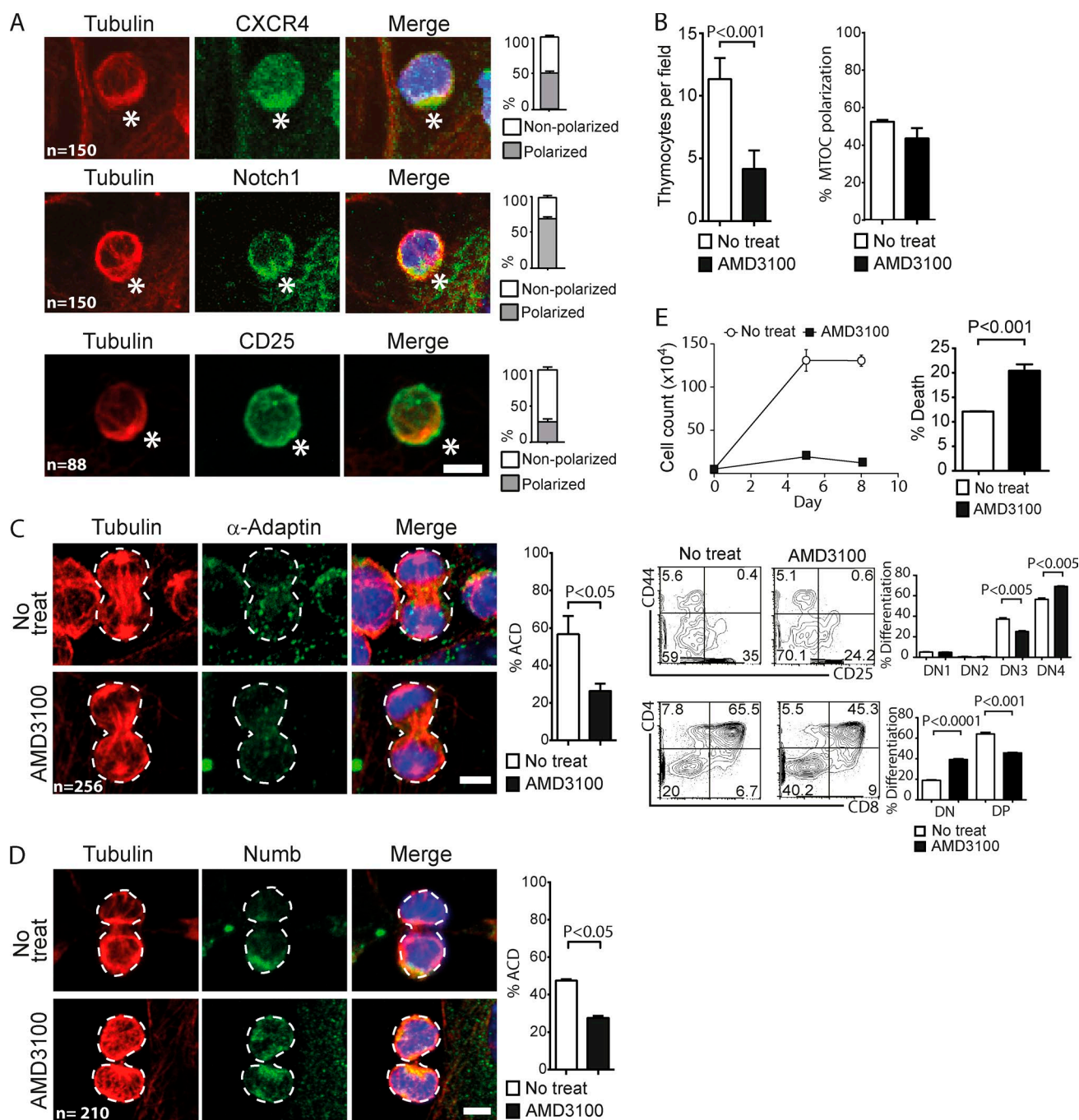


**Figure 3. Intact CXCR4 signaling constitutes a molecular requirement for DN3 thymocyte polarity during ACD.** (A) CXCR4 and Notch1, but not CD25, polarize to the stromal interface in DN3 thymocytes. Projected z stack images of DN3 thymocytes on OP9-DL1 stromal cells fixed and stained for  $\alpha$ -tubulin and either CXCR4, Notch1, or CD25. Percentage of thymocytes displaying nonpolarized localization if the protein of interest did not colocalize with the MTOC, or polarized localization if it localized with the MTOC at the thymocyte–stromal interface. The interface is indicated by the asterisks.  $n = 4$  independent experiments; total cells analyzed,  $n = 388$ . (B) CXCR4 signaling is required for DN3 thymocyte attachment to the stromal cell but not MTOC polarization. DN3 thymocytes were counted in randomly chosen fields of view (up to 25 fields of view). DN3 thymocytes that were still attached to a stromal cell (no treatment or with 2  $\mu$ g/ml AMD3100) were scored for thymocyte MTOC polarization to the thymocyte–stromal interface. An unpaired Student's  $t$  test ( $P < 0.05$ ) was used. (C and D) Inhibition of CXCR4 signaling reduces ACD in DN3 thymocytes as determined by loss of  $\alpha$ -Adaptin (C) and Numb asymmetry (D). Z-projected images were taken of DN3 thymocytes cultured on OP9-DL1 stromal cells (no treatment or with 2  $\mu$ g/ml AMD300) stained for  $\alpha$ -tubulin and  $\alpha$ -Adaptin or Numb. The percentage of ACD events, as determined by polarization of  $\alpha$ -Adaptin and Numb, are shown during DN3 division.  $n = 3$  independent experiments; total events,  $n = 256$  ( $\alpha$ -Adaptin) and 210 (Numb). An unpaired Student's  $t$  test ( $P < 0.05$ ) was used. (E) Intact CXCR4 signaling is required for downstream DN3 thymocyte cell numbers, survival, and differentiation. Sorted DN3 thymocytes were cultured on OP9-DL1 stromal cells (no treatment or 2  $\mu$ g/ml AMD3100) for up to 16 d and assessed for cell numbers, death by propidium iodide–positive staining, and differentiation from DN3 to the DP stage (the proportion of cells in each differentiation stage expressed as a percentage of DN [top plots] or total thymocytes [bottom plots] is shown in each quadrant for a single experiment and plotted as a bar graph for three combined experiments).  $n = 3$  independent experiments, with flow cytometry plots from one representative experiment shown. An unpaired Student's  $t$  test ( $P < 0.05$  and  $P < 0.001$ ) was used. The white dotted lines depict the outline of the dividing thymocyte. Bars, 10  $\mu$ m. All data are represented as  $\pm$ SEM.



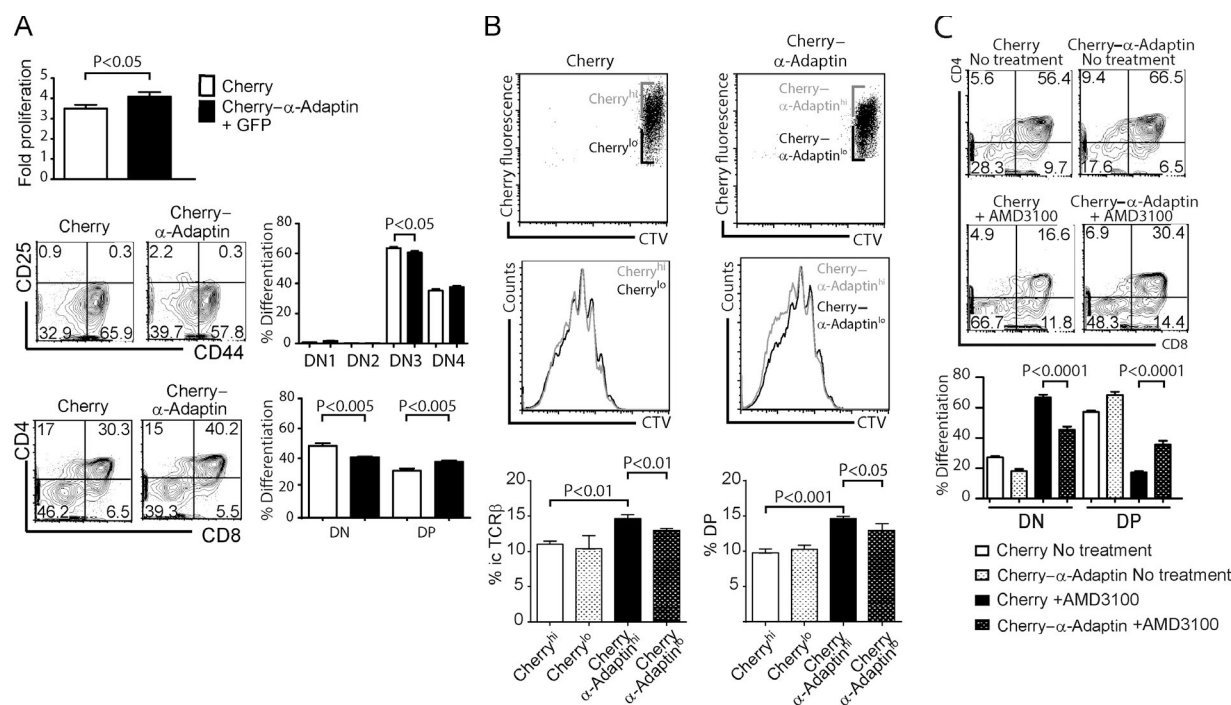


**Figure 4. Levels of  $\alpha$ -Adaptin correlate with functional differences in downstream DN3 fate.** (A) Overexpression of the endocytic molecule  $\alpha$ -Adaptin increases proliferation and differentiation of DN3 thymocytes to the DP stage. DN3 thymocytes expressing either Cherry or Cherry- $\alpha$ -Adaptin were sorted and cultured on OP9-DL1 stromal cells for 5 d. The fold proliferation and differentiation to DP was assessed (numbers in each quadrant of the flow cytometry dot plots represent the proportion of cells in each differentiation stage, expressed as a percentage of DN [top plots] and as a percentage of all thymocytes [bottom plots], and the mean of these proportions over seven independent experiments is represented in the bar graphs). Representative plots are shown from  $n = 7$  independent experiments. An unpaired Student's  $t$  test ( $P < 0.05$  and  $P < 0.001$ ) was used. (B) Cherry- $\alpha$ -Adaptin<sup>hi</sup> DN3a thymocytes undergo enhanced proliferation, signaling, and differentiation. Cherry and Cherry- $\alpha$ -Adaptin DN3a thymocytes labeled with CTV were cultured on OP9-DL1 stromal cells overnight. Daughters expressing hi or lo Cherry fluorescence (top) were sorted and recultured on OP9-DL1 stromal cells for 6 d and then assessed for proliferation (CTV dilution; middle) and intracellular (ic) TCR- $\beta$  (bottom) as a percentage of DN thymocytes, and differentiation to DP.  $n = 3$  independent experiments, with representative flow cytometry plots shown. An unpaired Student's  $t$  test was used ( $P < 0.05$  and  $P < 0.001$ ). (C) Ectopic expression of  $\alpha$ -Adaptin partially rescues blocks in DN3 thymocyte differentiation in the absence of CXCR4 signaling. Cherry and Cherry- $\alpha$ -Adaptin-sorted DN3 thymocytes were recultured on OP9-DL1 stromal cells for 6 d in the presence or absence of AMD3100 and then harvested for flow cytometry analysis. An unpaired Student's  $t$  test was performed to compare Cherry + AMD3100 versus Cherry- $\alpha$ -Adaptin + AMD3100 (DN and DP;  $P < 0.0001$ ; the proportion of each differentiation stage expressed as a percentage of total thymocytes [bottom plots] is displayed in each quadrant of the flow cytometry dot plots, and the mean of these values over four independent experiments is shown in the bar graphs below).  $n = 4$ , and representative replicates are shown. Data are represented as  $\pm$ SEM.

**$\alpha$ -Adaptin inheritance alters downstream thymocyte proliferation, signaling, and differentiation.**  $\alpha$ -Adaptin regulates hematopoietic stem cell self-renewal and segregates asymmetrically in dividing hematopoietic stem cells and sensory organ precursors of *D. melanogaster* (Berdnik et al., 2002; Ting et al., 2012).  $\alpha$ -Adaptin is best known as a regulator of endocytosis (Aguet et al., 2013), and it alters fate determination via effects on Notch and Numb trafficking during and after ACD (Smith and Chircop, 2012; Ting et al., 2012; Cotton et al., 2013; Couturier et al., 2013; Reichardt and Knoblich, 2013). Having identified  $\alpha$ -Adaptin as differentially inherited by the two daughters during ACD at the DN3a stage, we next assessed whether  $\alpha$ -Adaptin levels might also alter thymocyte fate. DN3 thymocytes ectopically expressing Cherry or Cherry- $\alpha$ -Adaptin were cultured on OP9-DL1 stromal cells for 5 d, and proliferation and differentiation were assessed. Cherry- $\alpha$ -Adaptin overexpression increased both thymocyte expansion and the proportion of thymocytes that differentiated from the DN3 to the DP stage (Fig. 4 A). These data indicate that increased levels of  $\alpha$ -Adaptin enhanced thymocyte expansion and differentiation.

To correlate levels of  $\alpha$ -Adaptin with downstream fate and to confirm the developmental stage at which  $\alpha$ -Adaptin exerts

its effects, Cherry or Cherry- $\alpha$ -Adaptin-expressing DN3a thymocytes were labeled with CTV to mark proliferation, and thymocytes that had undergone cell division were sorted for Cherry "hi" and "lo" fluorescence and cultured in equal numbers on OP9-DL1 stromal cells (Fig. 4 B, top and middle). After 6 d of culture, Cherry- $\alpha$ -Adaptin<sup>hi</sup> DN3a thymocytes had proliferated more than Cherry- $\alpha$ -Adaptin<sup>lo</sup> cells (Fig. 4 B, top and middle) and showed increased TCR signaling, as defined by increased levels of intracellular TCR- $\beta$  staining and enhanced differentiation to the next thymocyte stage (DP; Fig. 4 B, bottom). Differences in levels of  $\alpha$ -Adaptin expression in DN3a thymocytes can therefore influence proliferation and differentiation. To determine whether  $\alpha$ -Adaptin overexpression and CXCR4 signaling were functionally linked, we compared the effect of the CXCR4 inhibitor, AMD3100, on DN3a thymocytes expressing Cherry or Cherry- $\alpha$ -Adaptin. After 6 d, inhibition of CXCR4 signaling impeded the transition from double negative (DN) to DP (reduced from 56.4% DP to 16.6% DP; Fig. 4 C). In contrast, ectopic expression of  $\alpha$ -Adaptin increased differentiation to DP and partially rescued the differentiation defect, significantly increasing the proportion of CXCR4-inhibited DN3 thymocytes that reached the DP stage (from 16.6% to 30.4%;  $P < 0.0001$ ; Fig. 4 C). These data suggest that  $\alpha$ -Adaptin and CXCR4 func-

tionally interact to orchestrate polarization and differentiation or survival. CXCR4 appears to function upstream of  $\alpha$ -Adaptin because it provides a cue for  $\alpha$ -Adaptin polarization before division. Collectively, these data suggest the possibility that ACD of DN3a thymocytes might allow for populations with different levels of  $\alpha$ -Adaptin to influence fate choices such as proliferation and differentiation.

**Numb requires aPKC phosphorylation sites for polarity during DN3 division.** In a second approach to determine the functional relevance of ACD in thymocytes, we explored the effect on thymocyte fate of alterations in polarity of the cell fate determinant, Numb. We have previously shown that although ectopic expression of wild-type Numb has minimal impact on DN3 fate decisions (Aguado et al., 2010; Pham et al., 2013), expression of a mutated form of Numb (Numb2A) that lacks two serine substrates for phosphorylation by the polarity protein aPKC showed defective progression from DN3 to DP (Pham et al., 2013). aPKC regulates the polarization of Numb during ACD of many cell types including T cells (Oliaro et al., 2010), suggesting the possibility that aPKC might also regulate Numb polarization in DN3 cells to control DN3 fate decisions. Indeed, aPKC was polarized in  $\sim 12\%$  of dividing DN3 cells (Fig. 5 A). In contrast to wild-type Numb (12.7% ACD; Fig. 2 D), Numb2A was not polarized during division in DN3 thymocytes (4% scored as ACD compared with 4% in the control protein; Fig. 5 B). These results, combined with our previous finding that ectopic expression of Numb and Numb2A exerts different effects on DN3 fate (Pham et al., 2013), suggest that the asymmetric distribution of Numb during division of DN3 thymocytes is regulated by evolutionarily conserved mechanisms involving aPKC and that optimal progression from DN to DP requires asymmetric distribution of Numb.

**Scribble is required for polarity and optimal thymopoiesis.** In some examples of ACD, asymmetry of the Par3 complex (of which aPKC is a member) is regulated by antagonistic effects of the Scribble polarity complex, which includes Scribble, Dlg, and Lethal giant larvae (Albertson and Doe, 2003; Pham et al., 2014). However, staining for endogenous Scribble in dividing DN3 thymocytes showed little, if any, polarization during division (Fig. 6 A). Time-lapse imaging of ectopically expressed Scribble fused to GFP also showed little or no asymmetry, and PRs for GFP-Scribble and Cherry were not significantly different (Fig. 6 B). A previous study of *D. melanogaster* neuroblast ACD has shown that the Scribble complex is transiently polarized in early mitosis, disperses during telophase, but is crucial for mitotic spindle asymmetry and cortical polarity at division (Albertson and Doe, 2003). This precedent suggests that Scribble might regulate ACD of thymocytes by polarizing before division to influence the mitotic spindle and the polarity of cell fate determinants.

To assess whether polarization and T cell development required Scribble, we assessed thymocytes of mice in which the Scribble gene had been deleted in all cells (Pearson et al., 2011). Scribble<sup>-/-</sup> mice die before birth, so Ly5.1<sup>+</sup> mice were reconstituted with embryonic day (E) 13–14.5 Ly5.2<sup>+</sup> fetal liver cells from Scribble<sup>-/-</sup> embryos and wild-type littermate controls as performed previously (Hawkins et al., 2013). 12 wk after reconstitution, the proportion of thymocyte subpopulations was analyzed. The number of thymocytes (>95% donor derived) and the proportion of bulk DN, DP, single-positive (SP) CD4, and SP CD8 cells were all normal in Scribble<sup>-/-</sup> thy-

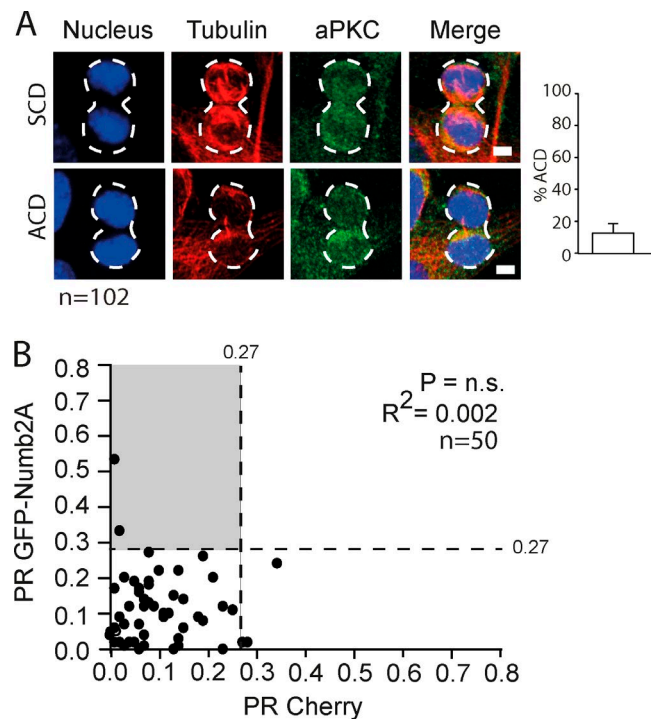


**Figure 5. Intact aPKC phosphorylation is required for polarization of Numb during DN3 division.** (A) aPKC polarization during DN3 thymocyte division. Z-projected images of dividing DN3 thymocytes cultured on OP9-DL1 stromal cells fixed and stained for  $\alpha$ -tubulin, DNA, and aPKC. The white dotted lines depict the outline of the dividing thymocyte. Images were scored as SCD or ACD based on blind assessment of aPKC fluorescence distribution. Scores as a percentage are shown.  $n = 3$ ; total cells analyzed,  $n = 102$ . Bars, 10  $\mu$ m. (B) Mutation of phosphorylated serine abrogates Numb asymmetry during DN3 thymocyte division. Absolute PR plots of dividing DN3 thymocytes expressing Cherry and GFP-Numb2A. Total divisions,  $n = 50$ . A paired  $t$  test comparing PR values for test and control protein and Pearson's linear correlation coefficient are shown. n.s., not significant.

mocytes (Fig. 6 C). However, Scribble<sup>-/-</sup> mice had increased DN4 cells (on average 58.6% more;  $P < 0.05$ ) despite having fewer DN2 cells than wild-type littermates (42.7% fewer;  $P < 0.005$ ; Fig. 6 D). The grossly normal T cell development is compatible with our earlier findings that Scribble depletion does not affect peripheral T cell composition or responses to infection (Hawkins et al., 2013), and the subtlety of the DN defect might reflect the fact that compensatory mechanisms frequently hamper phenotypic analysis of polarity-deficient mice, in which phenotypes are often only evident in very young mice or acute knockouts (Pham et al., 2014). We assessed whether the increase in DN4 thymocytes was compatible with an impact in changes in the proportion of cells undergoing ACD. We developed three mathematical models (described in Materials and methods section Mathematical models of thymocyte development . . . ) that can predict how asymmetry in dividing DN3a cells could impact the numbers of DN4 cells in the steady state. We took into account that DN3a cells can remain DN3a even after a cell division (Fig. S3 C) and that all DN3a cells must undergo at least one cell division before progressing to the DN4 stage (Kreslavsky et al., 2012). This implies that the first division is unique, as cells before this division are not permitted to differentiate, so two separate populations of DN3a cells were defined (termed DN3a-pre and DN3a-post) with the criteria that both populations could die and divide,



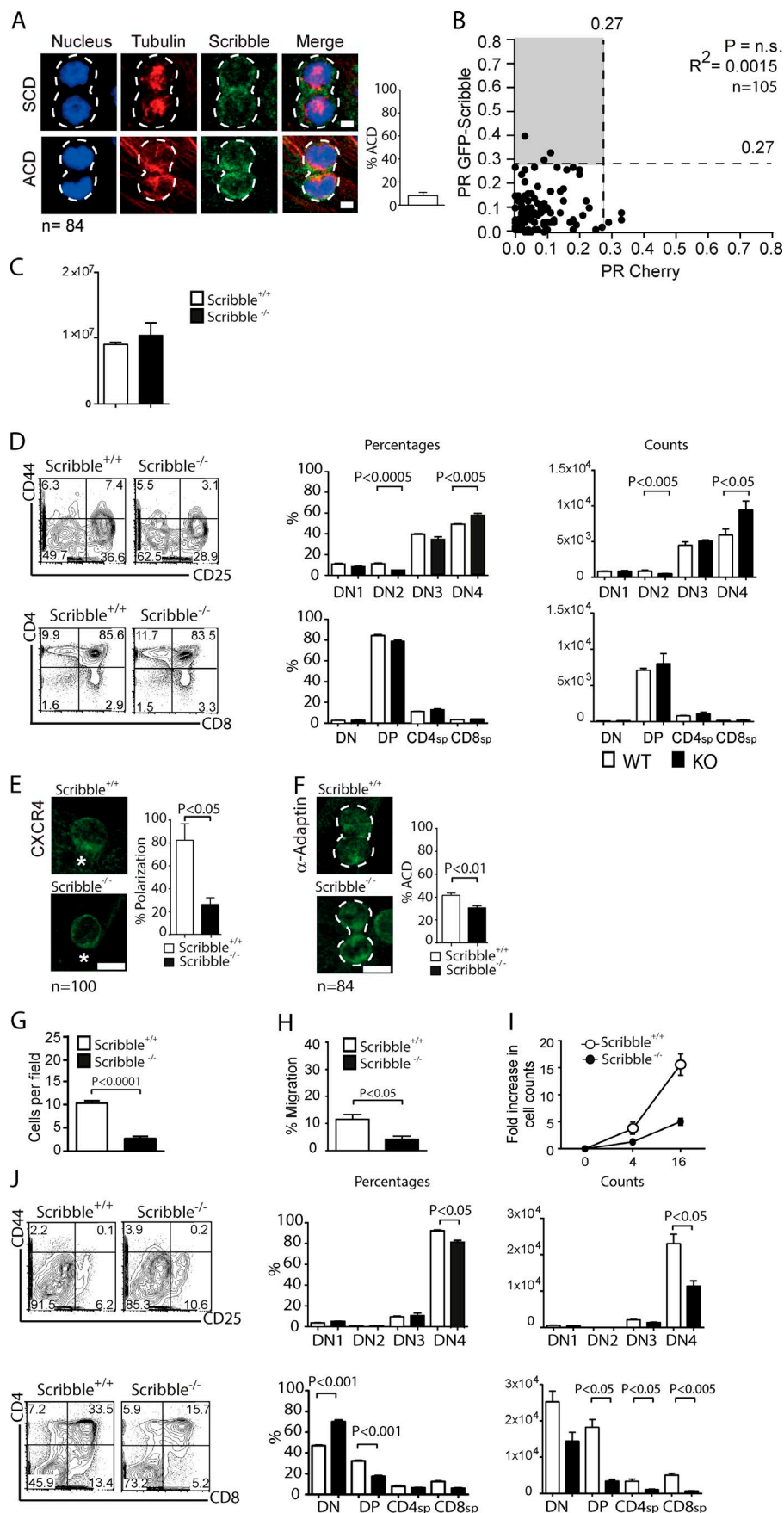


**Figure 6. In vivo and in vitro thymopoiesis is perturbed in the absence of Scribble.** (A) Scribble does not strongly polarize during DN3 thymocyte division. Representative z-projected images are shown of dividing DN3 thymocytes cultured on OP9-DL1 stromal cells fixed and stained for  $\alpha$ -tubulin, nucleus, and Scribble, with the percentage of SCD or ACD using  $\alpha$ -Adaptin as a marker.  $n = 4$ ; total divisions,  $n = 84$ . The white dotted lines depict the outline of the dividing thymocyte. (B) Little polarization of Scribble was observed during time-lapse imaging of dividing DN3 thymocytes. Paired  $t$  test of PR values and Pearson's linear regression coefficient ( $R^2$ ) are shown.  $n = 3$ ;  $n = 105$  divisions. (C and D) Scribble loss in vivo (C) does not alter gross thymocyte numbers but alters the balance of DN and DP cells in vivo. (D) Scribble $^{+/+}$  and Scribble $^{-/-}$  DN3a thymocytes were isolated from reconstituted mice and analyzed by flow cytometry for the proportions of DN, DP, and SP stages of differentiation. Numbers in each quadrant of the flow cytometry dot plots represent the proportion of cells in each differentiation stage, expressed as a percentage of DN (top plots) and as a percentage of all thymocytes (bottom plots), and the mean of these proportions over seven experiments is represented in the bar graphs. (E) Scribble is required for coordination of CXCR4-mediated polarity cues. Scribble $^{+/+}$  and Scribble $^{-/-}$  DN3a thymocytes were isolated, fixed, and stained for CXCR4 during interphase. Representative z-projected images are shown.  $n = 2$  independent experiments;  $n = 100$ . The white asterisks indicate the interface between the thymocyte and stromal cell. (F) Scribble is required for efficient DN3a ACD. Scribble $^{+/+}$  and Scribble $^{-/-}$  DN3a thymocytes were isolated, fixed, and stained for  $\alpha$ -Adaptin as a marker of asymmetry during division. Representative z-projected images are shown.  $n = 2$  independent experiments;  $n = 84$ . The white dotted lines depict the outline of the dividing thymocyte. (G) Scribble is required for DN3 thymocyte attachment to the stromal cell and asymmetric polarization of  $\alpha$ -Adaptin during division. DN3 thymocytes were counted in randomly chosen fields of view for up to 25 fields of view. DN3 thymocytes that were still attached to a stromal cell were scored for  $\alpha$ -Adaptin polarization as a marker for ACD.  $n = 3$ ; total cells analyzed,  $n = 84$ . (H) Loss of CXCL12-directed migration in the absence of Scribble. DN3 thymocytes were placed in Transwell plates containing 40 ng/ml SDF- $\alpha$ . The percent migrated shown is normalized to the BSA control.  $n = 3$ , and an unpaired Student's  $t$  test ( $P < 0.05$ ) was used. (I and J) Proliferation (I) and differentiation (J) of thymic progenitors on OP9-DL1 stromal cells are impeded in the absence of Scribble. Scribble $^{+/+}$  or Scribble $^{-/-}$  E14.5 fetal liver cells were cultured on OP9-DL1 stromal cells for 16 d and assessed for proliferation at 0, 4, and 16 d after culture, with differentiation at 16 d after culture shown. Numbers in each quadrant of the flow cytometry dot plots represent the proportion of cells in each differentiation stage, expressed as a percentage of DN (upper plots), and as a percentage of all thymocytes (lower plots), and the mean of these proportions over five independent experiments is represented in the bar graphs.  $n = 5$ . Data are shown as  $\pm$ SEM. KO, knockout; n.s., not significant; WT, wild type. Bars, 10  $\mu$ m.

but only the DN3a-post could differentiate. Assuming standard rules for rates of proliferation, death, and differentiation, we then modeled the impact on DN4 numbers in three scenarios: (1) divisions are symmetric, (2) ACD occurs at the DN3a-pre stage, and (3) ACD occurs at the DN3a-post stage (see Materials and methods section Mathematical models of thymocyte development . . . for details). Our mathematical analysis demonstrates that assuming the per cell proliferation rate of the DN3a-post cells is larger than their death rate, a decrease in the proportion of DN3a cells undergoing ACD observed in the *Scribble* knockout mice would lead to an increase in the number of DN4 cells in the steady state if the asymmetry occurred in the DN3a-post cells. The increased DN4 cells in the steady-state *Scribble* knockout mice would also be compatible with asymmetry in the DN3a-pre cells if the rate of death was greater than proliferation for DN3a cells. However, we suggest that this is an unlikely scenario because DN3a cells express high *Bcl2* levels and are protected from cell death (Voll et al., 2000). Of the three models, the data appear most consistent with ACD occurring in DN3a-post cells after an obligatory DN3a division. Elucidating this complex process will clearly require substantially more experimentation, but such mathematical models provide a robust framework to further explore the timing and effects of DN3a ACD.

To investigate T cell development in which steady-state T cell development had not yet been reached, progenitor cells from *Scribble*<sup>-/-</sup> E13–14.5 fetal liver were cultured on OP9-DL1 stromal cells. *Scribble*<sup>-/-</sup> DN3a thymocytes displayed several defects in polarity and migration: reduced polarization of CXCR4 in interphase from 82% to 26% ( $P < 0.05$ ; note that the polarization at interphase was also higher in DN3a cells than in the total DN3 cells assessed in Fig. 3 A, suggesting that DN3a cells exhibit greater polarity at all phases of the cell cycle; Fig. 6 E); reduced ACD as indicated by reduced polarization of  $\alpha$ -Adaptin from 41% to 30% ( $P < 0.01$ ; Fig. 6 F); reduced adherence to stromal cells from 10.3 cells to 2.7 thymocytes attached per field of view ( $P < 0.001$ ; Fig. 6 G); and 53.7% reduced migration across a membrane in response to the CXCR4 chemokine, CXCL12, in a Transwell assay ( $P < 0.05$ ; Fig. 6 H). To determine whether these alterations in polarity correlated with differences in fate, we cultured *Scribble*<sup>-/-</sup> fetal liver progenitors on OP9-DL1 stromal cells for 16 d to assess in vitro thymopoiesis. The most striking impact on the fate of the thymocytes was severely abrogated cell expansion (Fig. 6 I). At day 16, when most of the wild-type cells had progressed through the DN stages, *Scribble*<sup>-/-</sup> cells were impaired in their progression past DN3, and this was associated with a reduction in DP thymocytes (Fig. 6 J). Our findings are compatible with a previous study in which RNAi-mediated depletion of *Scribble* reduced cellularity and the DN3 to DP transition (Pike et al., 2011). These data indicate that *Scribble* is required for polarity during cell division and that loss of polarity correlates with altered expansion and differentiation of thymocytes both in vitro and in vivo.

## Discussion

We demonstrate that ACD occurs at the  $\beta$ -selection checkpoint during T cell development in thymocytes. Stromal cells and chemokines provide cues to DN3a cells that control the asymmetric distribution of Numb and  $\alpha$ -Adaptin during cell

division, and both ACD and subsequent fate are controlled by *Scribble* as has previously been shown in neuroblasts (Albertson and Doe, 2003). These findings indicate that ACD during T cell development uses conserved mechanisms that have previously been elucidated in cells of solid tissues and in mature T cells, providing clues as to the functional role of ACD during the  $\beta$ -selection checkpoint. Alterations in the polarity of Numb, alterations in inheritance of  $\alpha$ -Adaptin, the deletion of *Scribble*, and consequent reduction in ACD all correlate with changes in differentiation and proliferation of DN3 thymocytes. This indicates that ACD of DN3a thymocytes influences cell fate decisions (Fig. 7 A).

Why might DN3a cells undergo ACD? ACD at the  $\beta$ -selection checkpoint might regulate self-renewal and expansion at the level of the individual cell, mitigate the high risk of leukemia caused by combining gene rearrangement with subsequent expansion, and/or enable abrupt transitions in differentiation state and growth signal dependencies (Rothenberg, 2014). These possible roles are compatible with the role of the *Scribble* complex and ACD in other cell types (Martin-Belmonte and Perez-Moreno, 2012), where a switch between ACD and SCD can control subsequent differentiation and tumorigenesis (Morin and Bellaïche, 2011). Therefore, the extent of ACD could mediate control of thymocyte fate determination by stromal interactions and the strength of Notch and CXCR4 signaling. In addition, a switch from ACD to SCD after the  $\beta$ -selection checkpoint might enable a limited expansion of individual clones that are already destined for terminal differentiation.

We propose two nonmutually exclusive cellular processes by which ACD of DN3a cells might facilitate the balance of self-renewal and expansion of individual clones at the  $\beta$ -selection checkpoint (Fig. 7 B). (1) Studies have suggested that the limited proliferation of DN3a cells might facilitate expansion of a particular partial TCR rearrangement (Tourigny et al., 1997; Petrie et al., 2000). It has also been shown that DN3a cells absolutely require progression through the cell cycle to differentiate to DP, whereas DN3b cells are capable of differentiation without cell division (Dose et al., 2006; Kreslavsky et al., 2012). ACD in this context could allow one daughter to remain undifferentiated and perhaps self-renew, whereas the other differentiates and proliferates. Asymmetry in the first division of DN3a cells might release a brake on differentiation by segregating away fate determinants that inhibit differentiation. Our modeling suggests that DN3a ACD does not need to be restricted to this first division, but quantitative knowledge of proliferation and death rates is required to definitively assess this. (2) A second cellular process that could be controlled by ACD relates to apoptosis, analogous to *D. melanogaster* sensory organ precursors where the differential inheritance of Numb is regulated by ACD and leads to death of one of the daughters (Orgogozo et al., 2002). Before the  $\beta$ -selection checkpoint, thymocytes are protected from cell death by expression of *Bcl2*, but after  $\beta$  selection *Bcl2* is down-regulated, and apoptosis follows unless productive pre-TCR signaling induces expression of *Bcl2-A1*. Unlike *Bcl2*, *Bcl2-A1* does not delay proliferation (Mandal et al., 2005). Coordinating the change in susceptibility with chromosomal rearrangements and differentiation potential must be intricately orchestrated (Mandal et al., 2005; Aifantis et al., 2006; Kee, 2009), and ACD at the DN3a stage might enable partitioning of apoptosis regulators or their upstream signaling components to ensure appropriate apoptotic responses. One possibil-

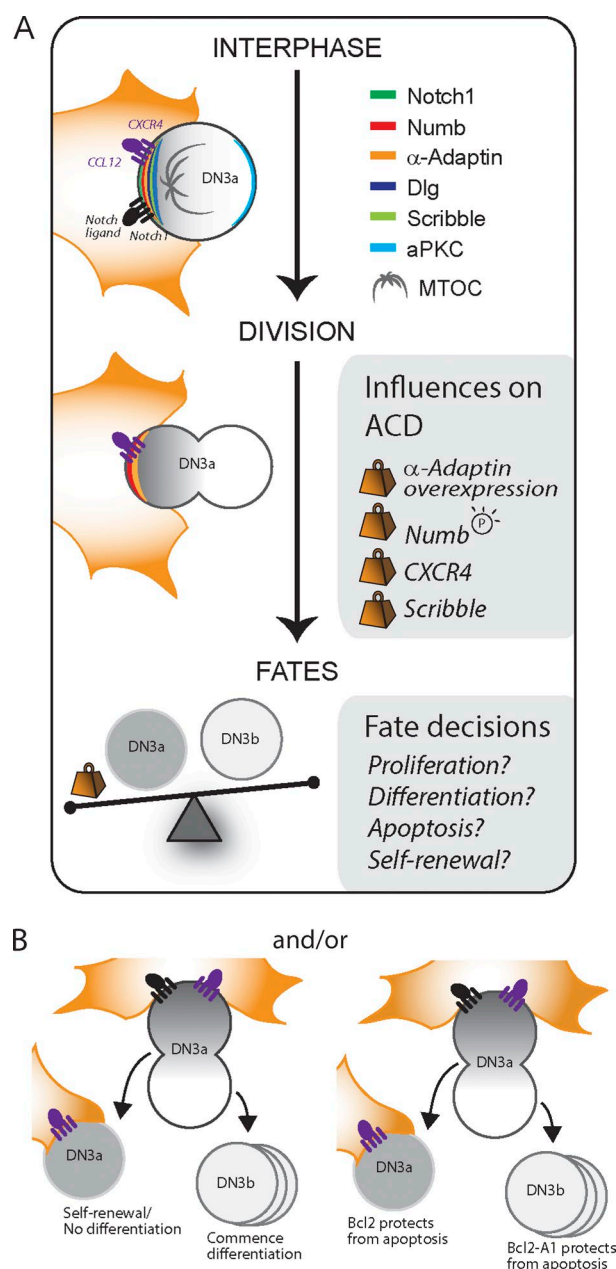


**Figure 7. A model for ACD of DN3a thymocytes.** (A) During interphase, engagement of the DN3a thymocyte with the stromal cell is mediated by CXCR4 and provides the cue for localization of several cell fate- and polarity-associated molecules, in particular  $\alpha$ -Adaptin and Numb, which also asymmetrically localize during division. Notch ligand interactions also provide important survival cues. ACD occurs preferentially when the cell divides perpendicularly to the stromal cell, indicating that cues from the stromal cell orchestrate the division. Inhibition of CXCR4 signaling, differential inheritance of  $\alpha$ -Adaptin, disruption in Numb phosphorylation, (circled P = phosphorylation) and Scribble deficiency all influence ACD and alter the balance of polarity, downstream proliferation, differentiation, apoptosis, and possibly self-renewal. (B) Two nonexclusive possible roles could exist for ACD of DN3a cells. (1) Niche availability might allow one DN3a thymocyte daughter cell to self-renew, whereas the other daughter cell commences differentiation. (2) Differential segregation of molecules (such as Bcl-2 and/or Bcl2-A1) into the daughters might orchestrate differential susceptibility to apoptosis. One or both of these immediate effects on cellular activities of the two daughter cells would differentially impact the probability and timing with which they progress to further differentiation and expansion.

ity is that such partitioning is mediated through  $\alpha$ -Adaptin and Numb, which are polarized in DN3 thymocytes and regulate endocytosis (Berdnik et al., 2002; Couturier et al., 2012). These two nonmutually exclusive processes would then set the stage for subsequent proliferation and progression through the final stages of thymocyte differentiation. The loss of ACD and striking effect on thymocyte proliferation upon deletion of Scribble supports such a role for ACD in coordinating proliferation and self-renewal. Thus, ACD of DN3a cells provides a potential means to reconcile the seemingly contradictory requirements of thymocyte development, enabling limited self-renewal and expansion alongside chromosomal rearrangement.

The finding that ACD is controlled by CXCR4 signaling and stromal interactions provides a mechanistic explanation for recent findings of the role for CXCR4 in thymocyte fate determination and that a stromal niche enables self-renewal of DN3 cells (Martins et al., 2012; Peaudecr et al., 2012). This is reminiscent of the competition for niches that regulates ACD and self-renewal of *D. melanogaster* germline stem cells (Losick et al., 2011). ACD can control fate by allowing only one daughter access to the niche, as in *D. melanogaster* ovarian germline cells (Losick et al., 2011), or can involve the asymmetric segregation of fate determinants as in *D. melanogaster* neuroblasts (Knoblich, 2010). Our findings indicate that the latter scenario is true in thymocytes, as fate determinants are asymmetrically distributed such that the daughters are molecularly distinct. However, this does not exclude the possibility that stromal access is also restricted to only one daughter. CXCR4 is required for survival of DN3 cells after  $\beta$  selection by induction of Bcl2-A1 (Janas et al., 2010; Trampont et al., 2010). In this instance, ACD of DN3a cells might allow induction of Bcl2-A1 by CXCR4 only in one of the daughters, leaving the other to inherit the remaining Bcl2 protein (Fig. 7 B). A recent finding that Bcl2 is down-regulated in older DN3 cells only under physiological conditions of cell competition within the thymic niche (Martins et al., 2014) provides support for the notion that ACD, restricted by interactions with stromal cells, induces differential susceptibility to apoptosis in DN3 progeny. Elucidating whether the two daughters exhibit differential self-renewal, susceptibility to apoptosis, differentiation, or cell divisions will require longitudinal analysis of cell differentiation, division, and death as cells progress beyond DN3a. However, the dramatic changes in proliferation observed in the Scribble-deficient cells in vitro, and the shifts in proportions of cells before and after the  $\beta$ -selection checkpoint both in vitro and in vivo, suggest that the alterations in fate of the DN3a progeny can profoundly impact the subsequent expansion of  $\beta$ -selected cells.

Together, these findings indicate that DN3a thymocytes undergo ACD to regulate downstream fate determination and begin to elucidate the mechanisms by which ACD is regulated. Interactions between the stromal cell and the DN3a thymocyte orchestrate polarity that is dependent on CXCR4 signaling. This interaction leads to polarization of the cell fate regulators Numb and  $\alpha$ -Adaptin and alignment of the polarity axis with the mitotic spindle to ensure their differential inheritance into the two daughter cells and subsequent differences in fate programming in each daughter cell. The tractability of experimental systems for the study of T cell development, combined with the rich knowledge of molecular pathways involved (Yui and Rothenberg, 2014), mean that this model system is likely to prove extremely useful for dissecting how ACD controls fate decisions.



## Materials and methods

### Primary thymocyte co-culture and mouse strains

E13.5–14.5 mouse fetal liver cells or bone marrow cells (isolated from C57BL/6 or littermate-matched *Scribble*<sup>−/−</sup> mice) were used as hematopoietic progenitors and seeded onto OP9-DL1 stromal cells (received from Juan-Carlos Zúñiga-Pflücker, University of Toronto, Sunnybrook Health Sciences Centre, Toronto, Ontario, Canada) at a 1:1 ratio in a 6-well plate ( $2 \times 10^5$ ) or a 12-well plate ( $10^5$ ) for differentiation of fetal liver cells into thymocytes in MEM Alpha modification supplemented with 10% vol/vol FCS, 1-nM L-glutamine, 50-μM β-mercaptoethanol, 1-nM sodium pyruvate, 10-mM Hepes, 100 ng/ml penicillin/streptomycin, 1 ng/ml mouse interleukin 7, and 5 ng/ml mouse Feline McDonough strain sarcoma virus-like tyrosine kinase 3. Thymocytes were harvested via forceful pipetting and co-cultured on freshly seeded OP9-DL1 stromal cells every 3–8 d. C57BL/6, B6-Ptprca, and *Scribble*<sup>−/−</sup> (C57BL/6 background) 6–12 wk old were used. All mice were maintained in a specific pathogen-free environment with food and water freely available. C57BL/6 and Ptprca mice were obtained from the Walter and Eliza Hall Institute of Medical Research animal breeding facility, and *Scribble* mice were obtained as described previously (Pearson et al., 2011). All experiments on mice were performed in accordance with the Animal Experimentation Ethics Committee of the Peter MacCallum Cancer Centre. For analysis of differentiation and proliferation, purified DN3 thymocytes were co-cultured on OP9-DL1 stromal cells and treated in the presence or absence of 2 μg/ml AMD3100 (Sigma-Aldrich) before harvesting and assessment of proliferation and differentiation by flow cytometric analysis of fixed confocal analysis.

### Retroviral transduction

Phoenix E cells (provided by Garry Nolan, Stanford University, Stanford, CA) were maintained at 37°C and at 10% CO<sub>2</sub> in Dulbecco's minimal essential medium supplemented with 10% vol/vol FCS and 1-mM L-glutamine. Calcium phosphate transfection was performed on Phoenix E cells with 5 μg of the following pMSCV retroviral constructs: Cherry, GFP, Cherry-tubulin, GFP-Numb, GFP-Numb2a, Cherry-α-Adaptin, and GFP-*Scribble* in 10-cm dishes (Corning). Viral supernatant was harvested 48 h after transfection, concentrated, and added to 6-well plates that had been precoated with 15 μg/ml RetroNectin (Takara Bio Inc.) and blocked in 2% BSA/PBS. After addition of the viral supernatant, plates were spun at 2,000 g for 1 h and incubated for 4 h at 37°C.  $1\text{--}4 \times 10^6$  bone marrow/E14.5 fetal liver cells or  $1\text{--}4 \times 10^6$  thymocytes (day 6–8 co-culture) were added, and plates were spun for 1 h at 1,200 g and sorted by flow cytometry after 24 h for live imaging, re-co-culture, or reconstitution into sublethally irradiated B6-Ptprca mice. For assessment of protein level inheritance by flow cytometry, transduced thymocytes were labeled with 2.5-μM CTV (Invitrogen) before flow cytometric sorting and culture on OP9-DL1 stromal cells.

### Flow cytometry

Retrovirally transduced cells were sorted on the basis of GFP or Cherry fluorescence on a FACS (FACSVantage; BD). DN3 thymocytes were isolated on the basis of surface expression (CD25<sup>+</sup>/CD44<sup>lo</sup>/CD4<sup>−</sup>/CD8<sup>−</sup>, lineage negative: Mac1<sup>−</sup>/CD3<sup>−</sup>/RB6-8C5<sup>−</sup>/NK1.1<sup>−</sup>/Ter119<sup>−</sup>), and DN3a and DN3b were further discriminated on the basis of CD28 expression (all antibodies were either anti-rat or anti-mouse and purchased from eBioscience or BD unless otherwise specified). DN3 or DN3a cells were also sorted for GFP or Cherry fluorescence if transduced. Proliferation and viability were analyzed by staining with CTV and Fluorogold, and/or thymocyte subsets were characterized by staining lineage negative (Mac1<sup>−</sup>/CD3<sup>−</sup>/RB6-8C5<sup>−</sup>/NK1.1<sup>−</sup>/Ter119<sup>−</sup>)

for the cell surface markers CD44/CD25 to determine the percentage of DN1–4 subsets, CD28 to determine the percentage of DN3a and DN3b, and CD4 and CD8 to determine the percentages of DN and DN and SP populations. Before antibody staining, Fc receptors were blocked by incubation with 2.4G2.

### Immunofluorescence and fixed image acquisition by confocal microscopy

$7 \times 10^3$  OP9 or OP9-DL1 stromal cells were seeded in each well of an 8-well chamber slide (Thermo Fisher Scientific) and left to adhere overnight.  $1\text{--}4 \times 10^4$  thymocytes were added with fresh media and co-cultured for 1–2 d. Cells were then fixed, permeabilized, and stained as previously described (Ludford-Menting et al., 2005). All cells were then labeled with primary antibodies as mentioned, labeled with secondary antibodies, and mounted in ProLong gold antifade (Molecular Probes). The slides were examined at room temperature using a confocal microscope (FluoView FV1000 BX61; Olympus) and a UIS2PlanApoN 60× 1.42 NA oil immersion objective. 3D images of the cells were acquired with a z distance of 0.5 μm. Maximum intensity projections of z sections spanning the entire cell were used for all analyses using FluoView software (version 1.7b; Olympus).

### Image acquisition and quantification using TACTICS software platform

DN3 thymocytes were seeded at a 1:1 ratio onto stromal cells ( $2 \times 10^4$  cells) in an 8-well chamber slide (ibidi) containing  $250 \times 250\text{-}\mu\text{m}$  cell paddocks pre-rinsed with ethanol and filled with MEM Alpha modification (Daniel Day, Swinburne University and Microsurfaces, Melbourne, Australia; Day et al., 2009). Multiple stage positions were acquired on a confocal microscope (TCS SP5 CLSM; Leica) using a 63× 1.3 NA glycerol immersion objective (corresponding to a pixel size of  $0.481 \times 0.481\text{ }\mu\text{m}$ ) for every 2 min for up to 24 h, with five-slice z stacks of 2–3-μm thickness taken at every time point. Thymocytes were imaged in a temperature-controlled chamber at 37°C with 10% CO<sub>2</sub> delivered to the chamber.

Images of the parent cell and daughters were used to create montages orientated along the major axis to enable qualitative assessment of fluorescence distribution. To quantify fluorescence in all divisions, we applied a PR equation to the thymocytes,  $PR = (\Sigma H1 - \Sigma H2)/(\Sigma H1 + \Sigma H2)$ , where the difference in total intensity between daughter 1 ( $\Sigma H1$ ) and daughter 2 ( $\Sigma H2$ ) was divided by the sum of intensities in both daughter 1 ( $H1$ ) and daughter 2 ( $H2$ ) one frame after division, similar to that previously described (Oliaro et al., 2010; Pham et al., 2013). However, as it was unknown which daughter thymocyte was  $H1$  or  $H2$  (i.e., proximal or distal), absolute PR values were taken to obtain PR values between 0 (completely symmetric) and 1 (completely asymmetric). Additionally, the control protein allowed control for differences in the focal plane for  $H1$  and  $H2$ . The PR values for the test proteins were plotted against the respective Cherry PR values for each division (Shimoni et al., 2014), and the significance was assessed using a paired *t* test.

### Transwell chemotaxis assay

24-well Transwell plates and 5-μm pore size inserts (Corning) were coated in 500 μl (plate) and 100 μl (insert) of 0.1% BSA/PBS overnight at 4°C. Plates and inserts were dried at room temperature before adding media (as described in the first Materials and methods section) containing either 40 μg/ml CXCL12/SDF1α (PeproTech) or 1% BSA.  $10^6$  sorted thymocytes (in 100 μl in the same media) were overlaid on top of each Transwell plate and allowed to migrate for 2 h at 37°C with 10% CO<sub>2</sub>, to which the percent migrated (output) was calculated as a proportion and fold change from the original input numbers of sorted thymocytes.

## Statistics

All data from flow cytometry, immunofluorescence staining, time-lapse microscopy, and mouse data were assumed to have normal distributions. Unpaired Student's  $t$  tests were performed with the exception of the PR scatterplots, in which paired  $t$  tests were performed between control and test PR values.

## Mathematical models of thymocyte development from DN3a to DP: SCD and ACD

### Experimental evidence that guides mathematical model development.

In this section, we introduce some hypotheses to build a mathematical model of the evolution of the populations of thymocytes (from DN3a to DP). These hypotheses are introduced in light of the experimental results of the manuscript. We consider the following five thymocyte populations. (1)  $x_a$  are DN thymocytes at stage 3a-pre describing the stage before the first DN3a division and so are not permitted to progress to DN4 (Kreslavsky et al., 2012). These cells die and divide but do not differentiate. (2)  $y_a$  are DN thymocytes at stage 3a-post. These cells originate from the 3a-pre thymocytes after one round of division. These cells die, divide, and differentiate into DN3b thymocytes. (3)  $x_b$  are DN thymocytes at stage 3b. These cells die, divide, and differentiate into DN4 thymocytes. (4)  $x_4$  are DN thymocytes at stage 4. These cells die, divide, and differentiate into DP thymocytes. (5)  $x_p$  are DP thymocytes. These cells die, divide, and differentiate into SP thymocytes (which are not included in the model).

**Cell death.** We assume all five populations can die (in principle): (1)  $x_a$  cells have a per cell death rate of  $\mu_a^{\text{pre}}$ ; (2)  $y_a$  cells have a per cell death rate of  $\mu_a^{\text{post}}$ ; (3)  $x_b$  cells have a per cell death rate of  $\mu_b$ ; (4)  $x_4$  cells have a per cell death rate of  $\mu_4$ ; and (5)  $x_p$  cells have a per cell death rate of  $\mu_p$ .

**Cell proliferation.** We assume the following proliferation rules.  $x_a$  cells can proliferate with a per cell rate of  $\lambda_a^{\text{pre}}$ . This proliferation event can be SCD (producing two daughter cells that are identical to each other but of type DN3a-post), or it can be ACD (producing one daughter cell that is identical to the mother cell, of type DN3a-pre, and a second daughter cell of type DN3a-post).  $y_a$  cells can proliferate with a per cell rate of  $\lambda_a^{\text{post}}$ . This proliferation event can be SCD (producing two daughter cells that are identical to the mother cell, of type DN3a-post), or it can be ACD (producing one daughter cell that is identical to the mother cell, of type DN3a-post, and a second daughter cell of type DN3b).  $x_b$  cells can proliferate with a per cell rate of  $\lambda_b$ . This proliferation event is assumed to be SCD (producing two daughter cells that are identical to the mother cell).  $x_4$  cells can proliferate with a per cell rate of  $\lambda_4$ . This proliferation event is assumed to be SCD (producing two daughter cells that are identical to the mother cell).  $x_p$  cells can proliferate with a per cell rate of  $\lambda_p$ . This proliferation event is assumed to be SCD (producing two daughter cells that are identical to the mother cell).

**Cell differentiation.** We assume the following differentiation rules.  $x_a$  cells are assumed not to be able to differentiate. They only die or proliferate.  $y_a$  cells differentiate to yield cells of type  $x_b$  with a per cell rate of  $\xi_a$ .  $x_b$  cells differentiate to yield cells of type  $x_4$  with a per cell rate of  $\xi_b$ .  $x_4$  cells differentiate to yield cells of type  $x_p$  with a per cell rate of  $\xi_4$ .  $x_p$  cells differentiate to yield cells of another type (SP), not considered in the model, with a per cell rate of  $\xi_p$ .

**Source term of DN3a-pre thymocytes.** We assume that DN3a-pre cells are generated from DN2 cells as follows: DN2 cells provide an overall flux of DN3a-pre cells (as they differentiate from DN2 to DN3a-pre) given by  $\varphi_a$  (number of cells per unit of time).

**Dynamical equations for the thymocyte populations. Model 1: SCDs only.** In this model, we assume that all divisions, at any stage of differentiation, are symmetric. In this case, the equations are given by

$$\frac{dx_a}{dt} = \varphi_a - \lambda_a^{\text{pre}} x_a - \mu_a^{\text{pre}} x_a,$$

$$\frac{dy_a}{dt} = 2 \lambda_a^{\text{pre}} x_a + \lambda_a^{\text{post}} y_a - \xi_a y_a - \mu_a^{\text{post}} y_a,$$

$$\frac{dx_b}{dt} = \xi_a y_a + \lambda_b x_b - \xi_b x_b - \mu_b x_b,$$

$$\frac{dx_4}{dt} = \xi_b x_b + \lambda_4 x_4 - \xi_4 x_4 - \mu_4 x_4,$$

and

$$\frac{dx_p}{dt} = \xi_4 x_4 + \lambda_p x_p - \xi_p x_p - \mu_p x_p.$$

**Model 2: One ACD (from DN3a-pre thymocytes).** In this model, we assume that all divisions (but one), at any stage of differentiation, are symmetric. We allow for ACD to take place when DN3a-pre thymocytes proliferate. In this case, the equations are given by

$$\frac{dx_a}{dt} = \varphi_a - \mu_a^{\text{pre}} x_a,$$

$$\frac{dy_a}{dt} = \lambda_a^{\text{pre}} x_a + \lambda_a^{\text{post}} y_a - \xi_a y_a - \mu_a^{\text{post}} y_a,$$

$$\frac{dx_b}{dt} = \xi_a y_a + \lambda_b x_b - \xi_b x_b - \mu_b x_b,$$

$$\frac{dx_4}{dt} = \xi_b x_b + \lambda_4 x_4 - \xi_4 x_4 - \mu_4 x_4,$$

and

$$\frac{dx_p}{dt} = \xi_4 x_4 + \lambda_p x_p - \xi_p x_p - \mu_p x_p.$$

**Model 3: One ACD (from DN3a-post thymocytes).** In this model, we assume that all divisions (but one), at any stage of differentiation, are symmetric. We allow for ACD to take place when DN3a-post thymocytes proliferate. In this case, the equations are given by

$$\frac{dx_a}{dt} = \varphi_a - \lambda_a^{\text{pre}} x_a - \mu_a^{\text{pre}} x_a,$$

$$\frac{dy_a}{dt} = 2 \lambda_a^{\text{pre}} x_a - \xi_a y_a - \mu_a^{\text{post}} y_a,$$

$$\frac{dx_b}{dt} = \lambda_a^{\text{post}} y_a + \zeta_a y_a + \lambda_b x_b - \zeta_b x_b - \mu_b x_b, \quad x_4^{*(\text{sym})} = \frac{\zeta_b}{(-\lambda_4 + \zeta_4 + \mu_4)} \frac{\zeta_a}{(-\lambda_b + \zeta_b + \mu_b)} \frac{2 \lambda_a^{\text{pre}}}{(-\lambda_a^{\text{post}} + \zeta_a + \mu_a^{\text{post}})} \frac{\varphi_a}{(\lambda_a^{\text{pre}} + \mu_a^{\text{pre}})},$$

$$\frac{dx_4}{dt} = \zeta_b x_b + \lambda_4 x_4 - \zeta_4 x_4 - \mu_4 x_4,$$

and

$$\frac{dx_p}{dt} = \zeta_4 x_4 + \lambda_p x_p - \zeta_p x_p - \mu_p x_p.$$

**Steady-state solutions and their stability. Model 1: SCDs only.** If we assume steady-state conditions, we obtain

$$0 = \varphi_a - \lambda_a^{\text{pre}} x_a - \mu_a^{\text{pre}} x_a,$$

$$x_a^{*(\text{sym})} = \frac{\varphi_a}{(\lambda_a^{\text{pre}} + \mu_a^{\text{pre}})},$$

$$0 = 2 \lambda_a^{\text{pre}} x_a + \lambda_a^{\text{post}} y_a - \zeta_a y_a - \mu_a^{\text{post}} y_a,$$

$$y_a^{*(\text{sym})} = \frac{2 \lambda_a^{\text{pre}} x_a^{*(\text{sym})}}{(-\lambda_a^{\text{post}} + \zeta_a + \mu_a^{\text{post}})},$$

$$y_a^{*(\text{sym})} = \frac{2 \lambda_a^{\text{pre}}}{(-\lambda_a^{\text{post}} + \zeta_a + \mu_a^{\text{post}})} \frac{\varphi_a}{(\lambda_a^{\text{pre}} + \mu_a^{\text{pre}})},$$

$$0 = \zeta_a y_a + \lambda_b x_b - \zeta_b x_b - \mu_b x_b,$$

$$x_b^{*(\text{sym})} = \frac{\zeta_a y_a^{*(\text{sym})}}{(-\lambda_b + \zeta_b + \mu_b)},$$

$$x_b^{*(\text{sym})} = \frac{\zeta_a}{(-\lambda_b + \zeta_b + \mu_b)} \frac{2 \lambda_a^{\text{pre}}}{(-\lambda_a^{\text{post}} + \zeta_a + \mu_a^{\text{post}})} \frac{\varphi_a}{(\lambda_a^{\text{pre}} + \mu_a^{\text{pre}})},$$

$$0 = \zeta_b x_b + \lambda_4 x_4 - \zeta_4 x_4 - \mu_4 x_4,$$

$$x_4^{*(\text{sym})} = \frac{\zeta_b x_b^{*(\text{sym})}}{(-\lambda_4 + \zeta_4 + \mu_4)},$$

$$0 = \zeta_4 x_4 + \lambda_p x_p - \zeta_p x_p - \mu_p x_p,$$

$$x_p^{*(\text{sym})} = \frac{\zeta_4 x_4^{*(\text{sym})}}{(-\lambda_p + \zeta_p + \mu_p)},$$

and

$$x_p^{*(\text{sym})} = \frac{\zeta_4}{(-\lambda_p + \zeta_p + \mu_p)} \frac{\zeta_b}{(-\lambda_4 + \zeta_4 + \mu_4)} \frac{\zeta_a}{(-\lambda_b + \zeta_b + \mu_b)} \frac{2 \lambda_a^{\text{pre}}}{(-\lambda_a^{\text{post}} + \zeta_a + \mu_a^{\text{post}})} \frac{\varphi_a}{(\lambda_a^{\text{pre}} + \mu_a^{\text{pre}})}.$$

The existence of this steady state requires the following conditions (on the parameters of the model):

$$-\lambda_a^{\text{post}} + \zeta_a + \mu_a^{\text{post}} > 0 \Rightarrow \zeta_a + \mu_a^{\text{post}} > \lambda_a^{\text{post}},$$

$$-\lambda_b + \zeta_b + \mu_b > 0 \Rightarrow \zeta_b + \mu_b > \lambda_b,$$

$$-\lambda_4 + \zeta_4 + \mu_4 > 0 \Rightarrow \zeta_4 + \mu_4 > \lambda_4,$$

and

$$-\lambda_p + \zeta_p + \mu_p > 0 \Rightarrow \zeta_p + \mu_p > \lambda_p.$$

We do not provide the details here, but it is easy to show that the previous conditions guarantee that the steady state defined by  $x_a^{*(\text{sym})}$ ,  $y_a^{*(\text{sym})}$ ,  $x_b^{*(\text{sym})}$ ,  $x_4^{*(\text{sym})}$ , and  $x_p^{*(\text{sym})}$  is a stable steady state.

**Model 2: One ACD (at the stage of DN3a-pre thymocytes).** If we assume steady-state conditions, we obtain

$$0 = \varphi_a - \mu_a^{\text{pre}} x_a,$$

$$x_a^{*(\text{asym2})} = \frac{\varphi_a}{\mu_a^{\text{pre}}},$$

$$0 = \lambda_a^{\text{pre}} x_a + \lambda_a^{\text{post}} y_a - \zeta_a y_a - \mu_a^{\text{post}} y_a,$$

$$y_a^{*(\text{asym2})} = \frac{\lambda_a^{\text{pre}} x_a^{*(\text{asym2})}}{(-\lambda_a^{\text{post}} + \zeta_a + \mu_a^{\text{post}})},$$

$$y_a^{*(\text{asym2})} = \frac{\lambda_a^{\text{pre}}}{(-\lambda_a^{\text{post}} + \zeta_a + \mu_a^{\text{post}})} \frac{\varphi_a}{\mu_a^{\text{pre}}},$$



$$0 = \zeta_a y_a + \lambda_b x_b - \zeta_b x_b - \mu_b x_b,$$

$$x_b^{*(\text{asym2})} = \frac{\zeta_a y_a^{*(\text{asym2})}}{(-\lambda_b + \zeta_b + \mu_b)},$$

$$x_b^{*(\text{asym2})} = \frac{\zeta_a}{(-\lambda_b + \zeta_b + \mu_b)} \frac{\lambda_a^{\text{pre}}}{(-\lambda_a^{\text{post}} + \zeta_a + \mu_a^{\text{post}})} \frac{\varphi_a}{\mu_a^{\text{pre}}},$$

$$0 = \zeta_b x_b + \lambda_4 x_4 - \zeta_4 x_4 - \mu_4 x_4,$$

$$x_4^{*(\text{asym2})} = \frac{\zeta_b x_b^{*(\text{asym2})}}{(-\lambda_4 + \zeta_4 + \mu_4)},$$

$$x_4^{*(\text{asym2})} = \frac{\zeta_b}{(-\lambda_4 + \zeta_4 + \mu_4)} \frac{\zeta_a}{(-\lambda_b + \zeta_b + \mu_b)} \frac{\lambda_a^{\text{pre}}}{(-\lambda_a^{\text{post}} + \zeta_a + \mu_a^{\text{post}})} \frac{\varphi_a}{\mu_a^{\text{pre}}},$$

$$0 = \zeta_4 x_4 + \lambda_p x_p - \zeta_p x_p - \mu_p x_p,$$

$$x_p^{*(\text{asym2})} = \frac{\zeta_4 x_4^{*(\text{asym2})}}{(-\lambda_p + \zeta_p + \mu_p)},$$

and

$$x_p^{*(\text{asym2})} = \frac{\zeta_4}{(-\lambda_p + \zeta_p + \mu_p)} \frac{\zeta_b}{(-\lambda_4 + \zeta_4 + \mu_4)} \frac{\zeta_a}{(-\lambda_b + \zeta_b + \mu_b)} \frac{\lambda_a^{\text{pre}}}{(-\lambda_a^{\text{post}} + \zeta_a + \mu_a^{\text{post}})} \frac{\varphi_a}{\mu_a^{\text{pre}}}.$$

The existence of this steady state requires the following conditions (on the parameters of the model):

$$-\lambda_a^{\text{post}} + \zeta_a + \mu_a^{\text{post}} > 0 \Rightarrow \zeta_a + \mu_a^{\text{post}} > \lambda_a^{\text{post}},$$

$$-\lambda_b + \zeta_b + \mu_b > 0 \Rightarrow \zeta_b + \mu_b > \lambda_b,$$

$$-\lambda_4 + \zeta_4 + \mu_4 > 0 \Rightarrow \zeta_4 + \mu_4 > \lambda_4,$$

and

$$-\lambda_p + \zeta_p + \mu_p > 0 \Rightarrow \zeta_p + \mu_p > \lambda_p.$$

We note that these conditions are the same as those required in the SCD model (model 1). Finally, we do not provide the details here, but it is easy to show that the previous conditions guarantee that

the steady state defined by  $x_a^{*(\text{asym2})}$ ,  $y_a^{*(\text{asym2})}$ ,  $x_b^{*(\text{asym2})}$ ,  $x_4^{*(\text{asym2})}$ , and  $x_p^{*(\text{asym2})}$  is a stable steady state.

**Model 3: One ACD (from DN3a-post thymocytes).** If we assume steady-state conditions, it is easy to show, as described in the previous two sections, that the steady state in this case is given by

$$x_a^{*(\text{asym3})} = \frac{\varphi_a}{\lambda_a^{\text{pre}} + \mu_a^{\text{pre}}},$$

$$y_a^{*(\text{asym3})} = \frac{2 \lambda_a^{\text{pre}}}{(\zeta_a + \mu_a^{\text{post}})} \frac{\varphi_a}{\lambda_a^{\text{pre}} + \mu_a^{\text{pre}}},$$

$$x_b^{*(\text{asym3})} = \frac{(\lambda_a^{\text{post}} + \zeta_a)}{(-\lambda_b + \zeta_b + \mu_b)} \frac{2 \lambda_a^{\text{pre}}}{(\zeta_a + \mu_a^{\text{post}})} \frac{\varphi_a}{\lambda_a^{\text{pre}} + \mu_a^{\text{pre}}},$$

$$x_4^{*(\text{asym3})} = \frac{\zeta_b}{(-\lambda_4 + \zeta_4 + \mu_4)} \frac{(\lambda_a^{\text{post}} + \zeta_a)}{(-\lambda_b + \zeta_b + \mu_b)} \frac{2 \lambda_a^{\text{pre}}}{(\zeta_a + \mu_a^{\text{post}})} \frac{\varphi_a}{\lambda_a^{\text{pre}} + \mu_a^{\text{pre}}},$$

and

$$x_p^{*(\text{asym3})} = \frac{\zeta_4}{(-\lambda_p + \zeta_p + \mu_p)} \frac{\zeta_b}{(-\lambda_4 + \zeta_4 + \mu_4)} \frac{(\lambda_a^{\text{post}} + \zeta_a)}{(-\lambda_b + \zeta_b + \mu_b)} \frac{2 \lambda_a^{\text{pre}}}{(\zeta_a + \mu_a^{\text{post}})} \frac{\varphi_a}{\lambda_a^{\text{pre}} + \mu_a^{\text{pre}}}.$$

The existence of this steady state requires the following conditions (on the parameters of the model):

$$-\lambda_b + \zeta_b + \mu_b > 0 \Rightarrow \zeta_b + \mu_b > \lambda_b,$$

$$-\lambda_4 + \zeta_4 + \mu_4 > 0 \Rightarrow \zeta_4 + \mu_4 > \lambda_4,$$

and

$$-\lambda_p + \zeta_p + \mu_p > 0 \Rightarrow \zeta_p + \mu_p > \lambda_p.$$

Finally, we do not provide the details here, but it is easy to show that the previous conditions guarantee that the steady state defined by  $x_a^{*(\text{asym3})}$ ,  $y_a^{*(\text{asym3})}$ ,  $x_b^{*(\text{asym3})}$ ,  $x_4^{*(\text{asym3})}$ , and  $x_p^{*(\text{asym3})}$  is a stable steady state.

**Model comparison. Models 1 and 2: Comparison between SCD and ACD at the DN3a-pre stage.** We introduce the following ratios:

$$r_a^{\text{pre}} = \frac{x_a^{*(\text{sym})}}{x_a^{*(\text{sym})} + x_a^{*(\text{asym2})}} = \frac{\mu_a^{\text{pre}}}{\lambda_a^{\text{pre}} + 2 \mu_a^{\text{pre}}} = \frac{1}{\frac{\lambda_a^{\text{pre}}}{\mu_a^{\text{pre}}} + 2} < \frac{1}{2},$$

$$r_a^{\text{post}} = \frac{y_a^{*(\text{sym})}}{y_a^{*(\text{sym})} + y_a^{*(\text{asym2})}} = \frac{2 \mu_a^{\text{pre}}}{\lambda_a^{\text{pre}} + 3 \mu_a^{\text{pre}}},$$

$$r_b = \frac{x_b^{*(\text{sym})}}{x_b^{*(\text{sym})} + x_b^{*(\text{asym2})}} = \frac{2 \mu_a^{\text{pre}}}{\lambda_a^{\text{pre}} + 3 \mu_a^{\text{pre}}},$$

$$r_4 = \frac{x_4^{*(\text{sym})}}{x_4^{*(\text{sym})} + x_4^{*(\text{asym2})}} = \frac{2\mu_a^{\text{pre}}}{\lambda_a^{\text{pre}} + 3\mu_a^{\text{pre}}}$$

and

$$r_p = \frac{x_p^{*(\text{sym})}}{x_p^{*(\text{sym})} + x_p^{*(\text{asym2})}} = \frac{2\mu_a^{\text{pre}}}{\lambda_a^{\text{pre}} + 3\mu_a^{\text{pre}}}$$

The previous equations indicate that if  $\lambda_a^{\text{pre}} > \mu_a^{\text{pre}}$ , then  $r_4 < 1/2$  and thus  $x_4^{*(\text{sym})} < x_4^{*(\text{asym2})}$ . Conversely, if  $\lambda_a^{\text{pre}} < \mu_a^{\text{pre}}$ , then  $r_4 > 1/2$  and thus  $x_4^{*(\text{sym})} > x_4^{*(\text{asym2})}$ . The experimental observations show that Scribble<sup>-/-</sup> mice have increased DN4 thymocyte counts when compared with wild-type littermates. That is, ACD events reduce the population of DN4 thymocytes when compared with a scenario in which only SCD events are allowed. Mathematically, this implies that  $x_4^{*(\text{sym})} > x_4^{*(\text{asym2})}$ , which can only hold if  $\lambda_a^{\text{pre}} < \mu_a^{\text{pre}}$ . This requires the (per cell) proliferation rate of DN3a-pre thymocytes to be smaller than their death rate. We note that this constraint is not the only one required. In order for the mathematical model to ensure the existence of a steady-state solution, the following constraints are also required (as discussed in the previous Model 1 and Model 2 sections):  $\xi_a + \mu_a^{\text{post}} > \lambda_a^{\text{post}}$ ,  $\xi_b + \mu_b > \lambda_b$ ,  $\xi_4 + \mu_4 > \lambda_4$ , and  $\xi_p + \mu_p > \lambda_p$ .

In summary, if ACD reduces DN4 thymocyte counts (as supported by the experimental work) and ACD takes places at the DN3a-pre stage, mathematical modeling predicts the following conditions on the parameters:  $\mu_a^{\text{pre}} > \lambda_a^{\text{pre}}$ ,  $\xi_a + \mu_a^{\text{post}} > \lambda_a^{\text{post}}$ ,  $\xi_b + \mu_b > \lambda_b$ ,  $\xi_4 + \mu_4 > \lambda_4$ , and  $\xi_p + \mu_p > \lambda_p$ .

**Models 1 and 3: Comparison between SCD and ACD at the DN3a-post stage.** We define the following ratios:

$$r_a^{\text{pre}} = \frac{x_a^{*(\text{sym})}}{x_a^{*(\text{sym})} + x_a^{*(\text{asym3})}} = \frac{1}{2},$$

$$r_a^{\text{post}} = \frac{y_a^{*(\text{sym})}}{y_a^{*(\text{sym})} + y_a^{*(\text{asym3})}} = \frac{z_a + \mu_a^{\text{post}}}{-\lambda_a^{\text{post}} + 2(z_a + \mu_a^{\text{post}})} > \frac{1}{2},$$

$$r_b = \frac{x_b^{*(\text{sym})}}{x_b^{*(\text{sym})} + x_b^{*(\text{asym3})}} = \frac{(z_a + \mu_b^{\text{post}})z_a}{\lambda_a^{\text{post}}(-\lambda_a^{\text{post}} + \mu_a^{\text{post}}) + 2z_a(z_a + \mu_a^{\text{post}})},$$

$$r_4 = \frac{x_4^{*(\text{sym})}}{x_4^{*(\text{sym})} + x_4^{*(\text{asym3})}} = \frac{(z_a + \mu_b^{\text{post}})z_a}{\lambda_a^{\text{post}}(-\lambda_a^{\text{post}} + \mu_a^{\text{post}}) + 2z_a(z_a + \mu_a^{\text{post}})},$$

and

$$r_p = \frac{x_p^{*(\text{sym})}}{x_p^{*(\text{sym})} + x_p^{*(\text{asym3})}} = \frac{(z_a + \mu_b^{\text{post}})z_a}{\lambda_a^{\text{post}}(-\lambda_a^{\text{post}} + \mu_a^{\text{post}}) + 2z_a(z_a + \mu_a^{\text{post}})}.$$

The previous results indicate that if  $\lambda_a^{\text{post}} > \mu_a^{\text{post}}$ , then  $r_4 > 1/2$  and thus  $x_4^{*(\text{sym})} > x_4^{*(\text{asym3})}$ . Conversely, if  $\lambda_a^{\text{post}} < \mu_a^{\text{post}}$ , then  $r_4 < 1/2$  and thus  $x_4^{*(\text{sym})} < x_4^{*(\text{asym3})}$ . If  $\lambda_a^{\text{post}} = \mu_a^{\text{post}}$ , the ratios are all equal to 1/2 and both models generate the same number of cells (Models 1 and 3). The experimental observations show that Scribble<sup>-/-</sup> mice have increased DN4 thymocyte counts when compared with wild-type littermates. That is, ACD events reduce the population of DN4 thymocytes when compared with a scenario in which only SCD events are allowed. Mathematically, this implies that  $x_4^{*(\text{sym})} > x_4^{*(\text{asym3})}$ , which can only

hold if  $\lambda_a^{\text{post}} > \mu_a^{\text{post}}$ . This requires the (per cell) proliferation rate of DN3a-post thymocytes to be larger than their death rate. We note that this constraint is not the only one required. In order for the mathematical model to ensure the existence of a steady-state solution, the following constraints are also required (as discussed in sections Model 1: SCDs only and Model 2: One ACD):  $\xi_a + \mu_a^{\text{post}} > \lambda_a^{\text{post}}$ ,  $\xi_b + \mu_b > \lambda_b$ ,  $\xi_4 + \mu_4 > \lambda_4$ , and  $\xi_p + \mu_p > \lambda_p$ .

In summary, if ACD reduces DN4 thymocyte counts (as supported by the experimental work) and ACD takes places at the DN3a-post stage, mathematical modeling predicts the following conditions on the parameters:  $\xi_a + \mu_a^{\text{post}} > \lambda_a^{\text{post}}$ ,  $\xi_b + \mu_b > \lambda_b$ ,  $\xi_4 + \mu_4 > \lambda_4$ , and  $\xi_p + \mu_p > \lambda_p$ .

### Online supplemental material

Fig. S1 shows that blinded qualitative or quantitative assessment yields similar information regarding the polarization during interphase in immunofluorescence experiments. Fig. S2 (related to Fig. 1) shows gene expression analysis of polarity and cell fate proteins in major thymocyte subsets, as derived from the Immgen database. Fig. S3 (related to Fig. 2) shows further examples of asymmetry during thymocyte division, shows how cutoff values to assign each division as ACD or SCD were derived, and shows the relationship between cell division and differentiation of DN3a cells as determined by CTV labeling and flow cytometry. Fig. S4 (related to Fig. 2) demonstrates, with time-lapse imaging of DN3 thymocytes transduced with Cherry-tubulin OP9-DL1 stromal cells, that DN3 thymocytes divide in a variety of orientations. Online supplemental material is available at <http://www.jcb.org/cgi/content/full/jcb.201502053/DC1>.

### Acknowledgments

We thank Juan Carlos Zúñiga-Pflücker (University of Toronto, Sunnybrook Health Sciences Centre, Toronto, Canada), for OP9 stromal cell lines, Daniel Day (Swinburne University of Technology, Hawthorn, Australia; and Microsurfaces Pty Ltd, Flemington, Australia) for the cell paddocks, Adam Poetter (Northcote High School, Northcote, Australia) for manual correction of segmentation and tracking of the time-lapse imaging, and Terry Speed (Walter and Eliza Hall Institute, Melbourne, Australia) for advice on the quantification of polarity. We thank Jacques Miller (Walter and Eliza Hall Institute) and Mohammed Yassin (Peter MacCallum Cancer Centre, Melbourne, Australia) for critical reading of this manuscript. We are grateful to the Peter MacCallum Cancer Centre Experimental Animal, Flow Cytometry Core, and Microscopy Core Facilities for expert technical assistance. This work was performed in part at the Biointerface Engineering Hub in the Victorian Node of the Australian National Fabrication Facility.

This work was funded by the Australian National Health and Medical Research Council (project grants and fellowships to E.D. Hawkins, J. Oliaro, S.B. Ting, P.O. Humbert, and S.M. Russell), the Human Frontier Science Program (grant RGP0049), the Australian Research Council (fellowship to S.M. Russell), the Australian Cancer Research Foundation (Cell Biology Program), and the Swiss National Science Foundation (grant P300P3\_154664/1 provided funds to M. Charnley). This work benefited from data assembled by the Immgen Consortium (Heng et al., 2008).

The authors declare no competing financial interests.

Submitted: 16 February 2015

Accepted: 31 July 2015

## References

- Aguado, R., N. Martin-Blanco, M. Caraballo, and M. Canelles. 2010. The endocytic adaptor Numb regulates thymus size by modulating pre-TCR signaling during asymmetric division. *Blood*. 116:1705–1714. <http://dx.doi.org/10.1182/blood-2009-10-246777>
- Aguet, F., C.N. Antonescu, M. Mettlen, S.L. Schmid, and G. Danuser. 2013. Advances in analysis of low signal-to-noise images link dynamin and AP2 to the functions of an endocytic checkpoint. *Dev. Cell*. 26:279–291. <http://dx.doi.org/10.1016/j.devcel.2013.06.019>
- Aifantis, I., M. Mandal, K. Sawai, A. Ferrando, and T. Vilimas. 2006. Regulation of T-cell progenitor survival and cell-cycle entry by the pre-T-cell receptor. *Immunol. Rev.* 209:159–169. <http://dx.doi.org/10.1111/j.0105-2896.2006.00343.x>
- Albertson, R., and C.Q. Doe. 2003. Dlg, Scrib and Lgl regulate neuroblast cell size and mitotic spindle asymmetry. *Nat. Cell Biol.* 5:166–170. <http://dx.doi.org/10.1038/ncb922>
- Arsenio, J., B. Kakaradov, P.J. Metz, S.H. Kim, G.W. Yeo, and J.T. Chang. 2014. Early specification of CD8<sup>+</sup> T lymphocyte fates during adaptive immunity revealed by single-cell gene-expression analyses. *Nat. Immunol.* 15:365–372. <http://dx.doi.org/10.1038/ni.2842>
- Barnett, B.E., M.L. Ciocca, R. Goenka, L.G. Barnett, J. Wu, T.M. Laufer, J.K. Burkhardt, M.P. Cancro, and S.L. Reiner. 2012. Asymmetric B cell division in the germinal center reaction. *Science*. 335:342–344. <http://dx.doi.org/10.1126/science.1213495>
- Berdnjk, D., T. Török, M. González-Gaitán, and J.A. Knoblich. 2002. The endocytic protein  $\alpha$ -Adaptin is required for numb-mediated asymmetric cell division in *Drosophila*. *Dev. Cell*. 3:221–231. [http://dx.doi.org/10.1016/S1534-5807\(02\)00215-0](http://dx.doi.org/10.1016/S1534-5807(02)00215-0)
- Blanpain, C., and E. Fuchs. 2014. Plasticity of epithelial stem cells in tissue regeneration. *Science*. 344:1242281. <http://dx.doi.org/10.1126/science.1242281>
- Buchholz, V.R., M. Flossdorf, I. Hensel, L. Kretschmer, B. Weissbrich, P. Gräf, A. Verschoor, M. Schiemann, T. Höfer, and D.H. Busch. 2013. Disparate individual fates compose robust CD8<sup>+</sup> T cell immunity. *Science*. 340:630–635. <http://dx.doi.org/10.1126/science.1235454>
- Chang, J.T., V.R. Palanivel, I. Kinjyo, F. Schambach, A.M. Intlekofer, A. Banerjee, S.A. Longworth, K.E. Vinup, P. Mrass, J. Oliaro, et al. 2007. Asymmetric T lymphocyte division in the initiation of adaptive immune responses. *Science*. 315:1687–1691. <http://dx.doi.org/10.1126/science.1139393>
- Chang, J.T., M.L. Ciocca, I. Kinjyo, V.R. Palanivel, C.E. McClurkin, C.S. Dejong, E.C. Mooney, J.S. Kim, N.C. Steinell, J. Oliaro, et al. 2011. Asymmetric proteasome segregation as a mechanism for unequal partitioning of the transcription factor T-bet during T lymphocyte division. *Immunity*. 34:492–504. <http://dx.doi.org/10.1016/j.immuni.2011.03.017>
- Ciofani, M., and J.C. Zúñiga-Pflücker. 2005. Notch promotes survival of pre-T cells at the  $\beta$ -selection checkpoint by regulating cellular metabolism. *Nat. Immunol.* 6:881–888. <http://dx.doi.org/10.1038/ni1234>
- Ciofani, M., T.M. Schmitt, A. Ciofani, A.M. Michie, N. Cuburu, A. Aublin, J.L. Maryanski, and J.C. Zúñiga-Pflücker. 2004. Obligatory role for cooperative signaling by pre-TCR and Notch during thymocyte differentiation. *J. Immunol.* 172:5230–5239. <http://dx.doi.org/10.4049/jimmunol.172.9.5230>
- Cotton, M., N. Benhra, and R. Le Borgne. 2013. Numb inhibits the recycling of Sanpodo in *Drosophila* sensory organ precursor. *Curr. Biol.* 23:581–587. <http://dx.doi.org/10.1016/j.cub.2013.02.020>
- Couturier, L., N. Vodovar, and F. Schweisguth. 2012. Endocytosis by Numb breaks Notch symmetry at cytokinesis. *Nat. Cell Biol.* 14:131–139. <http://dx.doi.org/10.1038/ncb2419>
- Couturier, L., K. Mazouni, and F. Schweisguth. 2013. Numb localizes to endosomes and controls the endosomal sorting of notch after asymmetric division in *Drosophila*. *Curr. Biol.* 23:588–593. <http://dx.doi.org/10.1016/j.cub.2013.03.002>
- Day, D., K. Pham, M.J. Ludford-Menting, J. Oliaro, D. Izon, S.M. Russell, and M. Gu. 2009. A method for prolonged imaging of motile lymphocytes. *Immunol. Cell Biol.* 87:154–158. <http://dx.doi.org/10.1038/icb.2008.79>
- Dose, M., I. Khan, Z. Guo, D. Kovalovsky, A. Krueger, H. von Boehmer, K. Khazaie, and F. Gounari. 2006. c-Myc mediates pre-TCR-induced proliferation but not developmental progression. *Blood*. 108:2669–2677. <http://dx.doi.org/10.1182/blood-2006-02-005900>
- Edgar, B.A. 2012. Intestinal stem cells: no longer immortal but ever so clever... *EMBO J.* 31:2441–2443. <http://dx.doi.org/10.1038/emboj.2012.133>
- Gérard, A., A.E. Mertens, R.A. van der Kammen, and J.G. Collard. 2007. The Par polarity complex regulates Rap1- and chemokine-induced T cell polarization. *J. Cell Biol.* 176:863–875. <http://dx.doi.org/10.1083/jcb.200608161>
- Gerlach, C., J.C. Rohr, L. Perié, N. van Rooij, J.W. van Heijst, A. Velds, J. Urbanus, S.H. Naik, H. Jacobs, J.B. Beltman, et al. 2013. Heterogeneous differentiation patterns of individual CD8<sup>+</sup> T cells. *Science*. 340:635–639. <http://dx.doi.org/10.1126/science.1235487>
- Hawkins, E.D., J. Oliaro, A. Kallies, G.T. Belz, A. Filby, T. Hogan, N. Haynes, K.M. Ramsbottom, V. Van Ham, T. Kinwell, et al. 2013. Regulation of asymmetric cell division and polarity by Scribble is not required for humoral immunity. *Nat. Commun.* 4:1801. <http://dx.doi.org/10.1038/ncomms2796>
- Heng, T.S., M.W. Painter, Immunological Genome Project Consortium, K. Elpek, V. Lukacs-Kornek, N. Mauermann, S.J. Turley, D. Koller, F.S. Kim, A.J. Wagers, et al. 2008. The Immunological Genome Project: networks of gene expression in immune cells. *Nat. Immunol.* 9:1091–1094. <http://dx.doi.org/10.1038/ni1008-1091>
- Janas, M.L., G. Varano, K. Gudmundsson, M. Noda, T. Nagasawa, and M. Turner. 2010. Thymic development beyond  $\beta$ -selection requires phosphatidylinositol 3-kinase activation by CXCR4. *J. Exp. Med.* 207:247–261. <http://dx.doi.org/10.1084/jem.20091430>
- Kee, B.L. 2009. E and ID proteins branch out. *Nat. Rev. Immunol.* 9:175–184. <http://dx.doi.org/10.1038/nri2507>
- King, C.G., S. Koehli, B. Hausmann, M. Schmalder, D. Zehn, and E. Palmer. 2012. T cell affinity regulates asymmetric division, effector cell differentiation, and tissue pathology. *Immunity*. 37:709–720. <http://dx.doi.org/10.1016/j.immuni.2012.06.021>
- Knoblich, J.A. 2010. Asymmetric cell division: recent developments and their implications for tumour biology. *Nat. Rev. Mol. Cell Biol.* 11:849–860. <http://dx.doi.org/10.1038/nrm3010>
- Koch, U., and F. Radtke. 2011. Mechanisms of T cell development and transformation. *Annu. Rev. Cell Dev. Biol.* 27:539–562. <http://dx.doi.org/10.1146/annurev-cellbio-092910-154008>
- Kreslavsky, T., M. Gleimer, M. Miyazaki, Y. Choi, E. Gagnon, C. Murre, P. Sicinski, and H. von Boehmer. 2012.  $\beta$ -Selection-induced proliferation is required for  $\alpha\beta$  T cell differentiation. *Immunity*. 37:840–853. <http://dx.doi.org/10.1016/j.immuni.2012.08.020>
- Li, R. 2013. The art of choreographing asymmetric cell division. *Dev. Cell*. 25:439–450. <http://dx.doi.org/10.1016/j.devcel.2013.05.003>
- Losick, V.P., L.X. Morris, D.T. Fox, and A. Spradling. 2011. *Drosophila* stem cell niches: a decade of discovery suggests a unified view of stem cell regulation. *Dev. Cell*. 21:159–171. <http://dx.doi.org/10.1016/j.devcel.2011.06.018>
- Ludford-Menting, M.J., J. Oliaro, F. Sacirbegovic, E.T. Cheah, N. Pedersen, S.J. Thomas, A. Pasam, R. Iazzolino, L.E. Dow, N.J. Waterhouse, et al. 2005. A network of PDZ-containing proteins regulates T cell polarity and morphology during migration and immunological synapse formation. *Immunity*. 22:737–748. <http://dx.doi.org/10.1016/j.immuni.2005.04.009>
- Mandal, M., C. Borowski, T. Palomero, A.A. Ferrando, P. Oberdoerffer, F. Meng, A. Ruiz-Vela, M. Ciofani, J.C. Zuniga-Pflucker, I. Screpanti, et al. 2005. The BCL2A1 gene as a pre-T cell receptor-induced regulator of thymocyte survival. *J. Exp. Med.* 201:603–614. <http://dx.doi.org/10.1084/jem.20041924>
- Martin-Belmonte, F., and M. Perez-Moreno. 2012. Epithelial cell polarity, stem cells and cancer. *Nat. Rev. Cancer*. 12:23–38. <http://dx.doi.org/10.1038/nrc3169>
- Martins, V.C., E. Ruggiero, S.M. Schlenger, V. Madan, M. Schmidt, P.J. Fink, C. von Kalle, and H.R. Rodewald. 2012. Thymus-autonomous T cell development in the absence of progenitor import. *J. Exp. Med.* 209:1409–1417. <http://dx.doi.org/10.1084/jem.20120846>
- Martins, V.C., K. Busch, D. Juraeva, C. Blum, C. Ludwig, V. Rasche, F. Lasitschka, S.E. Mastitsky, B. Brors, T. Hielscher, et al. 2014. Cell competition is a tumour suppressor mechanism in the thymus. *Nature*. 509:465–470. <http://dx.doi.org/10.1038/nature13317>
- Metz, P.J., J. Arsenio, B. Kakaradov, S.H. Kim, K.A. Remedios, K. Oakley, K. Akimoto, S. Ohno, G.W. Yeo, and J.T. Chang. 2015. Regulation of asymmetric division and CD8<sup>+</sup> T lymphocyte fate specification by protein kinase C $\zeta$  and protein kinase C $\lambda$ . *J. Immunol.* 194:2249–2259. <http://dx.doi.org/10.4049/jimmunol.1401652>
- Morin, X., and Y. Bellaïche. 2011. Mitotic spindle orientation in asymmetric and symmetric cell divisions during animal development. *Dev. Cell*. 21:102–119. <http://dx.doi.org/10.1016/j.devcel.2011.06.012>
- Oliaro, J., A. Pasam, N.J. Waterhouse, K.A. Browne, M.J. Ludford-Menting, J.A. Trapani, and S.M. Russell. 2006. Ligation of the cell surface receptor, CD46, alters T cell polarity and response to antigen presentation. *Proc. Natl. Acad. Sci. USA*. 103:18685–18690. <http://dx.doi.org/10.1073/pnas.0602458103>
- Oliaro, J., V. Van Ham, F. Sacirbegovic, A. Pasam, Z. Bomzon, K. Pham, M.J. Ludford-Menting, N.J. Waterhouse, M. Bots, E.D. Hawkins, et al.



2010. Asymmetric cell division of T cells upon antigen presentation uses multiple conserved mechanisms. *J. Immunol.* 185:367–375. <http://dx.doi.org/10.4049/jimmunol.0903627>
- Orgogozo, V., F. Schweisguth, and Y. Bellaïche. 2002. Binary cell death decision regulated by unequal partitioning of Numb at mitosis. *Development.* 129:4677–4684.
- Paridaen, J.T., and W.B. Huttner. 2014. Neurogenesis during development of the vertebrate central nervous system. *EMBO Rep.* 15:351–364. <http://dx.doi.org/10.1002/embr.201438447>
- Pearson, H.B., P.A. Perez-Mancera, L.E. Dow, A. Ryan, P. Tennstedt, D. Bogani, I. Elsum, A. Greenfield, D.A. Tuveson, R. Simon, and P.O. Humbert. 2011. SCRIB expression is deregulated in human prostate cancer, and its deficiency in mice promotes prostate neoplasia. *J. Clin. Invest.* 121:4257–4267. <http://dx.doi.org/10.1172/JCI158509>
- Peaudecerf, L., S. Lemos, A. Galgano, G. Krenn, F. Vasseur, J.P. Di Santo, S. Ezine, and B. Rocha. 2012. Thymocytes may persist and differentiate without any input from bone marrow progenitors. *J. Exp. Med.* 209:1401–1408. <http://dx.doi.org/10.1084/jem.20120845>
- Petrie, H.T., M. Tourigny, D.B. Burtrum, and F. Livak. 2000. Precursor thymocyte proliferation and differentiation are controlled by signals unrelated to the pre-TCR. *J. Immunol.* 165:3094–3098. <http://dx.doi.org/10.4049/jimmunol.165.6.3094>
- Pham, K., R. Shimoni, M.J. Ludford-Menting, C.J. Nowell, P. Lobachevsky, Z. Bomzon, M. Gu, T.P. Speed, C.J. McGlade, and S.M. Russell. 2013. Divergent lymphocyte signalling revealed by a powerful new tool for analysis of time-lapse microscopy. *Immunol. Cell Biol.* 91:70–81. <http://dx.doi.org/10.1038/icb.2012.49>
- Pham, K., F. Sacirbegovic, and S.M. Russell. 2014. Polarized cells, polarized views: asymmetric cell division in hematopoietic cells. *Front. Immunol.* 5:26. <http://dx.doi.org/10.3389/fimmu.2014.00026>
- Pike, K.A., S. Kulkarni, and T. Pawson. 2011. Immature T-cell clustering and efficient differentiation require the polarity protein Scribble. *Proc. Natl. Acad. Sci. USA.* 108:1116–1121. <http://dx.doi.org/10.1073/pnas.1018224108>
- Plotkin, J., S.E. Prockop, A. Lepique, and H.T. Petrie. 2003. Critical role for CXCR4 signaling in progenitor localization and T cell differentiation in the postnatal thymus. *J. Immunol.* 171:4521–4527. <http://dx.doi.org/10.4049/jimmunol.171.9.4521>
- Real, E., S. Faure, E. Donnadieu, and J. Delon. 2007. Cutting edge: atypical PKCs regulate T lymphocyte polarity and scanning behavior. *J. Immunol.* 179:5649–5652. <http://dx.doi.org/10.4049/jimmunol.179.9.5649>
- Reichardt, I., and J.A. Knoblich. 2013. Cell biology: Notch recycling is numbered. *Curr. Biol.* 23:R270–R272. <http://dx.doi.org/10.1016/j.cub.2013.03.013>
- Rothenberg, E.V. 2014. Transcriptional control of early T and B cell developmental choices. *Annu. Rev. Immunol.* 32:283–321. <http://dx.doi.org/10.1146/annurev-immunol-032712-100024>
- Schmitt, T.M., and J.C. Zúñiga-Pflücker. 2002. Induction of T cell development from hematopoietic progenitor cells by delta-like-1 in vitro. *Immunity.* 17:749–756. [http://dx.doi.org/10.1016/S1074-7613\(02\)00474-0](http://dx.doi.org/10.1016/S1074-7613(02)00474-0)
- Shimoni, R., K. Pham, M. Yassin, M. Gu, and S.M. Russell. 2013. TACTICS, an interactive platform for customized high-content bioimaging analysis. *Bioinformatics.* 29:817–818. <http://dx.doi.org/10.1093/bioinformatics/btt035>
- Shimoni, R., K. Pham, M. Yassin, M.J. Ludford-Menting, M. Gu, and S.M. Russell. 2014. Normalized polarization ratios for the analysis of cell polarity. *PLoS ONE.* 9:e99885. <http://dx.doi.org/10.1371/journal.pone.0099885>
- Simons, B.D., and H. Clevers. 2011. Strategies for homeostatic stem cell self-renewal in adult tissues. *Cell.* 145:851–862. <http://dx.doi.org/10.1016/j.cell.2011.05.033>
- Smith, C.M., and M. Chircop. 2012. Clathrin-mediated endocytic proteins are involved in regulating mitotic progression and completion. *Traffic.* 13:1628–1641. <http://dx.doi.org/10.1111/tra.12001>
- Thaunat, O., A.G. Granja, P. Barral, A. Filby, B. Montaner, L. Collinson, N. Martinez-Martin, N.E. Harwood, A. Bruckbauer, and F.D. Batista. 2012. Asymmetric segregation of polarized antigen on B cell division shapes presentation capacity. *Science.* 335:475–479. <http://dx.doi.org/10.1126/science.1214100>
- Ting, S.B., E. Deneault, K. Hope, S. Cellot, J. Chagraoui, N. Mayotte, J.F. Dorn, J.P. Laverdure, M. Harvey, E.D. Hawkins, et al. 2012. Asymmetric segregation and self-renewal of hematopoietic stem and progenitor cells with endocytic Ap2a2. *Blood.* 119:2510–2522. <http://dx.doi.org/10.1182/blood-2011-11-393272>
- Tourigny, M.R., S. Mazel, D.B. Burtrum, and H.T. Petrie. 1997. T cell receptor (TCR)- $\beta$  gene recombination: dissociation from cell cycle regulation and developmental progression during T cell ontogeny. *J. Exp. Med.* 185:1549–1556. <http://dx.doi.org/10.1084/jem.185.9.1549>
- Tramont, P.C., A.C. Tosello-Tramont, Y. Shen, A.K. Duley, A.E. Sutherland, T.P. Bender, D.R. Littman, and K.S. Ravichandran. 2010. CXCR4 acts as a costimulator during thymic beta-selection. *Nat. Immunol.* 11:162–170. <http://dx.doi.org/10.1038/ni.1830>
- Verzi, M.P., and R.A. Shivdasani. 2010. Stem cells: The intestinal-crypt casino. *Nature.* 467:1055–1056. <http://dx.doi.org/10.1038/4671055a>
- Voll, R.E., E. Jimi, R.J. Phillips, D.F. Barber, M. Rincon, A.C. Hayday, R.A. Flavell, and S. Ghosh. 2000. NF- $\kappa$ B activation by the pre-T cell receptor serves as a selective survival signal in T lymphocyte development. *Immunity.* 13:677–689. [http://dx.doi.org/10.1016/S1074-7613\(00\)00067-4](http://dx.doi.org/10.1016/S1074-7613(00)00067-4)
- Wu, M., H.Y. Kwon, F. Rattis, J. Blum, C. Zhao, R. Ashkenazi, T.L. Jackson, N. Gaiano, T. Oliver, and T. Reya. 2007. Imaging hematopoietic precursor division in real time. *Cell Stem Cell.* 1:541–554. <http://dx.doi.org/10.1016/j.stem.2007.08.009>
- Xavier, R., S. Rabizadeh, K. Ishiguro, N. Andre, J.B. Ortiz, H. Wachtel, D.G. Morris, M. Lopez-Illasaca, A.C. Shaw, W. Swat, and B. Seed. 2004. Discs large (Dlg1) complexes in lymphocyte activation. *J. Cell Biol.* 166:173–178. <http://dx.doi.org/10.1083/jcb.200309044>
- Yamamoto, R., Y. Morita, J. Oehara, S. Hamaoka, M. Onodera, K.L. Rudolph, H. Ema, and H. Nakauchi. 2013. Clonal analysis unveils self-renewing lineage-restricted progenitors generated directly from hematopoietic stem cells. *Cell.* 154:1112–1126. <http://dx.doi.org/10.1016/j.cell.2013.08.007>
- Yui, M.A., and E.V. Rothenberg. 2014. Developmental gene networks: a triathlon on the course to T cell identity. *Nat. Rev. Immunol.* 14:529–545. <http://dx.doi.org/10.1038/nri3702>
- Zimdahl, B., T. Ito, A. Blevins, J. Bajaj, T. Konuma, J. Weeks, C.S. Koehlein, H.Y. Kwon, O. Arami, D. Rizzieri, et al. 2014. Lis1 regulates asymmetric division in hematopoietic stem cells and in leukemia. *Nat. Genet.* 46:245–252. <http://dx.doi.org/10.1038/ng.2889>